

CZECH TECHNICAL UNIVERSITY IN PRAGUE

Faculty of Mechanical Engineering

Department of Process Engineering

Master's Thesis



**EXPERIMENTAL STAND FOR OBSERVATION
OF A SUSPENSION FLOW IN A PIPE**

Academic year 2021-2022

Supervisor
Ing. Jiri Moravec, Ph.D.

Author
Harish Balakrishnan



MASTER'S THESIS ASSIGNMENT

I. Personal and study details

Student's name: **Balakrishnan Harish** Personal ID number: **490759**
Faculty / Institute: **Faculty of Mechanical Engineering**
Department / Institute: **Department of Process Engineering**
Study program: **Mechanical Engineering**
Branch of study: **Process Engineering**

II. Master's thesis details

Master's thesis title in English:

Experimental stand for observation of a suspension flow in a pipe

Master's thesis title in Czech:

Experimentální zařízení pro pozorování toku suspenze v trubce

Guidelines:

- Carry out a literature study in the field of measuring of velocity, temperature and concentration profiles in a suspension flowing in a pipe. Describe the existing methods of measurements and their properties.
- Based on the literature search make a design proposal of experimental stand, which could be used for measuring of required properties of suspension flow. Detail specification of all the necessary parts should be a part of the proposal (vessels for suspension preparation and storage, pipes, sensors, pumps - if needed, support system, etc.).
- The final version of the proposed experimental stand must have a form of compact functional unit. Each particular part must be fully specified (dimensions, ranges of measurements of each sensor, available flowrates and pressures, etc.). The parameters of suspensions will be specified by the supervisor.

Bibliography / sources:

According to the recommendation of Thesis supervisor

Name and workplace of master's thesis supervisor:

Ing. Jiří Moravec, Ph.D., Department of Process Engineering, FME

Name and workplace of second master's thesis supervisor or consultant:

Date of master's thesis assignment: **18.10.2021** Deadline for master's thesis submission: **07.01.2022**

Assignment valid until: **18.09.2022**

Ing. Jiří Moravec, Ph.D.
Supervisor's signature

prof. Ing. Tomáš Jikout, Ph.D.
Head of department's signature

prof. Ing. Michael Valášek, DrSc.
Dean's signature

III. Assignment receipt

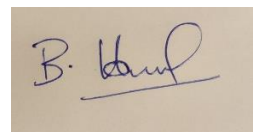
The student acknowledges that the master's thesis is an individual work. The student must produce his thesis without the assistance of others, with the exception of provided consultations. Within the master's thesis, the author must state the names of consultants and include a list of references.

25/10/2021
Date of assignment receipt

Student's signature

I confirm that the diploma work was disposed by myself and independently, under leading of my thesis supervisor. I stated all source of the documents and literature.

In Prague , 5/01/2022

A rectangular box containing a handwritten signature in blue ink. The signature appears to be 'B. Harish' with a horizontal line underneath.

BALAKRISHNAN HARISH

Acknowledgement

I would like to sincerely acknowledge to my supervisor, Ing. Jiri Moravec Ph.D., for his guidance and interest throughout this thesis. Thank you for your professional feedback, which encouraged me in improving my ideas in order to finish this project.

I would also like to thank my family for the sacrifice, support, patience and care they always gave to me. Thanks to everyone who believed in me, especially my girlfriend Natalia Bozikova, who encouraged me when I needed it the most. Without your help, I wouldn't have been able to finish.

Annotation sheet

Name: Harish

Surname: Balakrishnan

Title Czech: Experimentální zařízení pro pozorování toku suspenze v trubce

Title English: Experimental stand for observation of a suspension flow in a pipe

Scope of work: Number of pages: 73

Number of figures: 33

Number of tables: 7

Number of appendices: 10

Academic year: 2021/2022

Language: English

Department: Mechanical Engineering

Specialization: Process Engineering

Supervisor: Ing. Jiri Moravec, Ph.D.

Reviewer:

Submitter: Czech Technical University in Prague. Faculty of Mechanical Engineering,
Department of Process Engineering.

Annotation Czech: V práci byla zpracována literární rešerše zaměřená na zařízení pro měření rychlostních, koncentračních a teplotních profilů. Na základě rešerše bylo navrženo experimentální zařízení, které umožní měřit požadované parametry v suspenzi s balotinou proudící potrubím. Zařízení je navrženo tak, aby bylo přenosné, snadno rozšiřitelné a jsou u něj detailně definovány všechny parametry (rozměry, měřicí rozsahy senzorů, průtoky, tlaky, ventily a konstrukční části).

Annotation English: A review of the literature is conducted for a device that measures velocity, concentration, and temperature profile. The measurement instrument must be capable of measuring the requisite attributes of a glass bead particle suspended in water while flowing through a pipe. An experimental stand is constructed to measure the required qualities based on a literature search. Finally, the planned experimental stand should be portable in size, with all elements clearly described (dimensions, sensor measurement ranges, flowrates, pressure, valves, and constructional parts).

Keywords: Multiphase flow, Slurry flow, Terminal deposition velocity, Gravitational, Pumping, Double pipe heat exchanger, Shell and tube heat exchanger, Jacketed vessel mixing.

Utilization: For Department of Process Engineering, Czech Technical University in Prague

Table of Contents

Acknowledgement	iii
Annotation sheet	iv
List of Figures	ix
List of Tables	x
List of Abbreviations	xvii
ABSTRACT.....	xviii
INTRODUCTION	1
Chapter I – Multiphase Flow Measurement Techniques	4
1. Slurry flow in pipes	4
1.2. Slurry flow regimes in horizontal pipes	4
2. Measuring techniques of velocity and concentration profile	7
2.1. Laser Doppler Anemometry (LDA)	7
2.2. Particle Image Velocimetry (PIV).....	8
2.3. Positron Emission Particle Tracking (PEPT)	9
2.4. Pulsed Ultrasonic Doppler Velocimetry (PUDV)	11
2.5. Gamma ray and X-ray tomography.....	12
2.6. Electrical tomography technology.....	13
2.6.1. Electrical Impedance Tomography (EIT)	13
2.6.2. Electrical Capacitance Tomography (ECT).....	14
2.6.3. Electro Magnetic Tomography (EMT)	15
2.6.4. Electrical Resistance Tomography (ERT)	16
2.7. Magnetic Resonance Imaging (MRI)	17
3. Temperature Profile Measurement Techniques	18
3.1. Thermochromic Liquid Crystals (TLC)	18
3.2. Infrared Thermography (IRT)	19

3.3. Magnetic Resonance Thermometry (MRT)	20
3.4. Laser Induced Fluorescence (LIF).....	20
Chapter II – Calculation of limiting suspension parameters.....	22
1. Low concentrated suspension of fine particles of 10 microns with 5 V/V% solid concentration	22
1.1. Calculation of velocity	23
1.2. Mixing tank calculation.....	24
1.3. Pressure calculation.....	25
2. High concentrated suspension of coarse particles 2 mm with 30 V/V % of Solid concentration	26
Chapter III – Gravitational Method	27
1. Gravitational flow	27
1.1. Frictional losses	27
1.2. Mixing tank height from bottom	30
1.3. Pump calculation	30
1.3.1. Frictional losses in pipe, fittings, and valves	31
1.4. Pump power.....	31
1.5. Net positive suction head (NPSH).....	33
Chapter IV – Pumping Method.....	34
1. Pumping flow	34
1.1. Frictional losses in pipe, fittings, and valves.....	34
1.2. Pump power.....	35
1.3. Calculation of minimum speed of impeller (N_{js})	37
1.4. Shaft diameter calculation	39
1.5. Net positive suction head (NPSH).....	40
Chapter V – Heating units	42

1. Double pipe heat exchanger	42
2. Shell and tube heat exchanger	48
3. Jacket vessel heating	53
Chapter VI – Experimental stand for flow suspension in pipe flow.....	59
1.Experimental setup of slurry flow loop layout.....	59
2.Horizontal slurry flow loop layout.....	59
3. List of devices present inside experimental setup of slurry flow loop layout.....	60
3.1. Mixing tank	60
3.2 Supporting system	61
3.3. Centrifugal pump.....	62
3.4. Motor for mixing and pumping	63
3.5. Variable frequency drive	64
3.6. Pressure transmitter	64
3.7. Electromagnetic flow rate meter	65
3.8. Diaphragm valve	67
3.9. Temperature measurement	68
4. List of constructional components for flow loop	69
Result and discussion	70
Conclusion and Recommendation.....	72
References	74
Appendices.....	81

List of Figures

Figure 1 Forces acting on particles [32]	2
Figure 2 Homogenous flow [46].....	5
Figure 3 Heterogenous flow [46].....	6
Figure 4 Moving bed flow [46].....	6
Figure 5 Stationary bed flow [46].....	7
Figure 6 Laser Doppler Anemometry [48]	8
Figure 7 Particle Image Velocimetry [49]	9
Figure 8 Positron Emission Particle Tracking [50]	11
Figure 9 Pulsed Ultrasonic Doppler Velocimetry [51].....	11
Figure 10 Gamma ray and X -Ray Tomography [52]	13
Figure 11 Electrical Impedance Tomography [53].....	14
Figure 12 Electrical Capacitance Tomography [54].....	15
Figure 13 Electric Magnetic Tomography [55]	16
Figure 14 Electrical Resistance Tomography [56]	17
Figure 15 Magnetic Resonance Tomography [57]	18
Figure 16 Friction factor graph [32]	29
Figure 17 Mixing tank height	30
Figure 18 Simple pumping circuit	36
Figure 19 Power number vs Reynolds Number [58]	38
Figure 20 Double pipe heat exchanger [59].....	42
Figure 21 Shell and Tube heat exchanger [60]	48
Figure 22 Jacketed vessel	53
Figure 23 Overall Experimental setup [47]	60
Figure 24 Mixing tank with jacketed.....	61
Figure 25 Halfen stand for pipeline system.....	62
Figure 26 Warman slurry pump [61]	63
Figure 27 ABB- Flange mounted & Foot mounted motor [62].....	64
Figure 28 ABB - Variable frequency drive [62].....	64
Figure 29 Danfoss pressure transmitter [63].....	65
Figure 30 Siemens electromagnetic flowrate meter [64].....	66
Figure 31 Siemen's transmitter [64]	66

Figure 32 Straight diaphragm valve [65].....	67
Figure 33 K - type thermocouple [66]	68

List of Tables

Table 1 Frictional losses for valves and fittings [32].....	27
Table 2 Motor Specification [62].....	63
Table 3 Pressure Transmitter specification [63]	65
Table 4 Electromagnetic Flowrate Meter Specification [64].....	66
Table 5 Transmitter Specification [64]	66
Table 6 Diaphragm valve Specification [65]	67
Table 7 Constructional Component for flow loop	69

Nomenclature

A_1, A_w	Area of inner tube	m^2
A_2, A_s	Area of outer tube	m^2
A_m	Area of tank	m^2
a	Thermal diffusivity of water	m/s^2
C	Impeller clearance	m
C_D	Drag coefficient	–
C_w	Weight concentration of solids	%
C_v	Volume fraction of slurry	–
C_{pw}	Specific heat capacity of water	$kJ/kg\ K$
d	Diameter of shaft	m
d_p	Diameter of glass bead	m
D_a	Diameter of pitch blade agitator	m
D_e	Internal diameter of shell & tube exchanger	m
D_1	Inner diameter of tube	m
D_2	Outer diameter of tube	m
D_{in}	Inner diameter of tank	m
D_o	Outer diameter of tank	m
$\sum e_z$	Total frictional loss	J/kg
e_{zs}	Frictional loss at suction side	J/kg
F	Drag force	N
F_v	Buoyant force	N
F_s	Inertial force	N

f	Fanning friction factor	–
G	Gravitation force	N
g	Gravity constant	m/s ²
H	Total height	m
H_c	Height of cylinder	m
H_L	Liquid level	m
H_t	Height of Toro spherical	m
h_1, h_2	Vertical height	m
h_e	latent heat of steam	kJ/kg
h_{sh}	Static head	m
K	Safety factor	–
k^*	Relative roughness of pipe	–
k_{av}	Absolute roughness of pipe	mm
K_f	Frictional loss	J/kg
L	Total length	m
l_1	Unloading length of shaft	m
m_s, m_b	Mass flow rate of slurry	kg/s
m_{st}	Mass flow rate of steam	kg/s
m	Total mass of slurry	kg
M_k	Blade torque	Nm
M_0	Bending moment	Nm
M_{km}	Nominal Torque	Nm
M_{red}	Reduced Torque	Nm

N_{js}	Minimum speed of impeller	rpm
Nu	Nusselt number	—
N_t	No of tubes	—
N_a	Average number of tubes in row	—
n	Spindle speed	rpm
P	Pump power	kW
P_b	Pressure at tank bottom	Pa
P_T	Tube pitch	mm
Pr	Prandtl number	—
P_m	Power consumption	W
P_o	Power number	—
P_{vp}	Vapor pressure	Pa
P_{atm}	Atmospheric pressure	Pa
Q_v	Volumetric flow rate	m ³ /s
Q	Heat duty rate	kW
Re	Reynolds number	—
R_{steel}	Thermal resistance of steel	K/W
R_{water}	Thermal resistance of water side	K/W
R_{steam}	Thermal resistance of steam side	K/W
R_{Total}	Total thermal resistance	K/W
S_{in}	Inner surface area tank	m ²
S_o	Outer surface area tank	m ²
S_p	Specific surface of glass bead	m ²

S	Zwietering's constant	—
t	Heating time	s
T	Saturated water at average temperature	°C
T_s	Steam temperature	°C
T_w	Wall temperature	°C
T_2	Outlet temperature	°C
T_1	Inlet temperature	°C
u	Velocity of flow	m/s
U	Overall heat transfer coefficient	W/m ² K
V_D	Deposition velocity	m/s
V_t	Volume of tori spherical	m ³
v_t	Terminal Velocity	m/s
V_c	Volume of dished end	m ³
V	Volume of slurry	m ³
V_1	Initial velocity	m/s
W_s	Mechanical shaft work	J/kg
W_p	Mechanical pump work	J/kg
W_{weaker}	Thermal resistance of weaker energy stream	K/W

Greek Symbols

α	Flow regime	—
α_w	Heat transfer coefficient of water	W/m ² K
α_s	Heat transfer coefficient of steam	W/m ² K
λ	Friction factor	—
λ_w	Thermal conductivity of water	W/m. K
λ_s	Thermal conductivity of stainless steel	W/m. K
λ_{st}	Thermal conductivity of steam	W/m. K
Δ_{hv}	Vapor enthalpy	kJ/kg
Δ_{hl}	Liquid enthalpy	kJ/kg
Δ_{hvl}	Liquid vapor enthalpy	J/kg
ρ_l	Density of water	kg/ m ³
ρ_g	Density of glass bead particles	kg/ m ³
ρ_m	Bulk density of slurry	kg/ m ³
ρ_v	Density of steam	kg/ m ³
μ_l	Dynamic viscosity of water	Pa. s
μ_s	Dynamic viscosity of steam	Pa. s
μ_m	Viscosity of slurry	Pa. s
ΔT	Temperature difference	°C
ΔT_m	Mean logarithmic temperature difference	°C
γ	Baffled angle	°
ν	Kinematic viscosity of water	m ² /s
ϵ	Heat exchanger effectiveness	—

ξ	Konakov coefficient	—
σ_{kt}	Yield strength	MPa
η	Pump efficiency	—
ΔL	Overall length of pipe	m
ΔP_z	Pressure drops	Pa
ψ_p	Empirical correlation	—

List of Abbreviations

LDA	Laser Doppler Anemometry
PIV	Particle Image Velocimeter
CCD	Charged Coupled Device
PEPT	Positron Emission Particle Tracking
PUDV	Pulsed Ultrasonic Doppler Velocimetry
EIT	Electrical Impedance Tomography
ECT	Electrical Capacitance Tomography
EMT	Electro Magnetic Tomography
ERT	Electrical Resistance Tomography
MRI	Magnetic Resonance Imaging
TLC	Thermochromic Liquid Crystals
IRT	Infrared Thermography
MRT	Magnetic Resonance Thermometry
MRC	Magnetic Resonance Concentration
MRV	Magnetic Resonance Velocity
LIF	Laser Induced Fluorescence
LSF	Laser Stimulated Fluorescence
DPIT	Digital Particle Image Thermometry
CCC	Closed Circuit Camera
RGB	Red Green Blue

ABSTRACT

This project aims to develop a theoretical model and an experimental stand for measuring the velocity, concentration, and temperature profile of multiphase (liquid-solid) flow. Therefore, the literature study discusses the different measurement equipment and finally compares with each other for the precise equipment for the better profile. In this thesis, the measuring equipment is based on non-invasive technique methods.

The particles examined are glass beads with different volume concentrations (5 and 30 V/V %) and diameter (10 microns and 2 mm). The overall experimental stand should not exceed more than 10 meters in length.

An elaborate calculation report has been made for glass beads of two different volume concentrations and diameters based on the parameters (mixing tank, heating units, flow method, pump, motor, shaft, and impeller) used in the experimental stand. The calculation part is done using MS Excel.

After that, a comprehensive theoretical investigation was implemented to establish an appropriate detail specification of all parameters used for the experimental stand.

To make each parameter into individual 3D components, SOLID WORKS 2016 is used to make the components realistic, and AutoCAD 2019 is used to make a proper flow loop layout. The software used is licensed for students.

Finally, when all parameters satisfy the required condition, the individual components are assembled in a flow loop layout with all measurement sensors, pump, motors, valves, support stand, mixing tank, and other construction parts.

INTRODUCTION

Multiphase flow is a phenomenon that is ubiquitous in many industrial applications (oil, food, chemical and mining) and it describes the simultaneous flow of two or more phases in one system. In the chemical and mining industry, multiphase flow appears from mixing to the separator. Using the liquid and solid flow in one system is quite a challenging method for measuring the flow. Solid-liquid flow is also called a slurry flow. Slurry flow is very complex to design and analyze.

In this thesis, initially the water at 20 °C with glass bead particles are heated with the help of a jacketed vessel to reach the required temperature, 80 °C and the jacketed vessel coupled with pitch blade impeller for the suspension of the glass beads with water to make a slurry mixture. This type of initial heating is done when a jacketed vessel is used. There are two possible ways of heating by the jacketed vessel. One is simultaneously heating and mixing the slurry mixture and the other when it reaches the required temperature and after that, mixing can be started to reduce the power consumption of mixing during the heating. However, there are other types of heating device such as the double pipe and the shell & tube heat exchanger is explained in this work. During this type of heat exchanger, initially the slurry is mixed and then heated with the help of heat exchanger. To obtain a homogeneous mixture during flow, a motor is mounted concentrically to the mixing tank coupled to an agitator shaft and the speed of the motor is controlled by a variable frequency drive.

When there is a homogeneous mixture of slurry, the valves are opened to flow through the loop for the experimental test. During the flow of the slurry mixture, due to gravity the glass beads tend to settle at the bottom of the pipe. Since the glass bead particles have approximately two times higher density than water. This process of settling by gravity is called sedimentation and it takes some time for settling, it also depends on the velocity of the fluid or particle size. To avoid the glass beads from settling during the flow, the terminal deposition velocity of the slurry is determined. The forces that affect these particles during the settling are gravitational force, buoyant force, inertial force due to acceleration and drag force as shown in Figure 1.

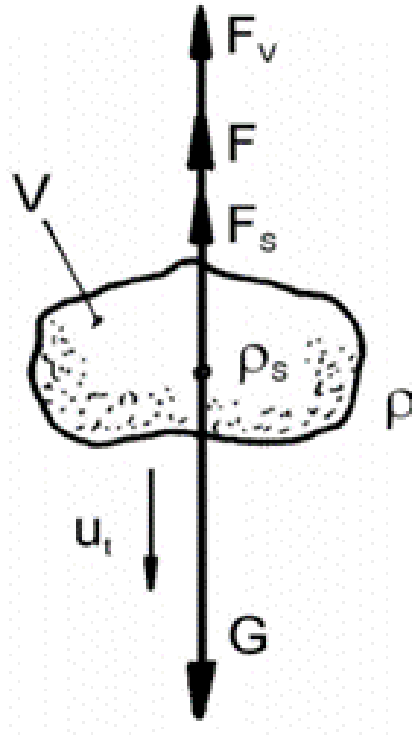


Figure 1 Forces acting on particles [32]

The balance equation of forces acting on the particle:

$$G - F_v - F_s - F = 0 \quad (1.1)$$

Gravitation force G can be expressed as:

$$G = V\rho_s g$$

Buoyant force F_v can be expressed as:

$$F_v = V\rho_l g$$

Inertial force due to acceleration F_s can be expressed as:

$$F_s = V\rho_s \frac{du_t}{dt}$$

Drag force F can be expressed as:

$$F = C_D S_p \rho_l \frac{V_D^2}{2}$$

In this work, two different types of experimental stand setup are mentioned. One method is based on gravitational flow without any external source like pump. The second method is based

on the pumping method with the help of an external source like pump coupled to a motor electrically connected with variable drive frequency.

The slurry mixture flows in the closed-circuit loop, when there is a change in flow rate, it is monitored by an electromagnetic flow rate meter. Similarly, when there is a pressure loss inside the flow, then it is monitored by the pressure transmitter. Therefore, once the measurement profiles are measured, the slurry flows into the storage tank and again the process repeats.

Chapter I – Multiphase Flow Measurement Techniques

1. Slurry flow in pipes

Slurry flow is a mixture of solid particles in a carrier liquid. The liquid is classified as a continuous flow, whereas solid particles are classified as a dispersed phase. The carrier fluid may be Newtonian or non-Newtonian. Water is used primarily as a carrier fluid in many industrial sectors. Solid particles are transported for bulk storage or to monitor physical and chemical processes in the flow. Due to the configuration of the pipe (horizontal, vertical, inclined), particle size, solid density, liquid density, solid shape, mean slurry velocity, pipe diameter, flow direction, liquid viscosity, and solid viscosity, the flow regime or patterns during slurry transportation become complex. The authors of the work [1] proposed a wide variety of experimental data has been reported in the literature on the relationship between particle size, deposition velocity and concentration. Basically, the flow is determined by particle size and concentration. To keep all these parameters in check, proper measurements should be taken to avoid pipe blockage due to settling. According to the study [2], most of the slurry pipelines flow within a limited range of mean velocities close to optimal. Gravity works perpendicular to the flow, and hence settling occurs mostly in horizontal flows. Gravity works against the dynamic force in the vertical flow, causing a slip velocity. In [3] it is reported that there are two essential aspects of solid transportation by liquids the resistance that solids will exert called drag force and the capacity of the liquid to lift such solids called lift force.

1.2. Slurry flow regimes in horizontal pipes

The study of the work [4] reported that the gravitational force acting on the particles complicates the flow of the slurry in the pipeline and causes different flow regimes. In slurry flow, the pressure drop is considered the most critical parameter. When compared to a pure liquid flow, the relationship between the pressure gradient and the mixing velocity is significantly different. In [67] the author developed one of the most important classifications for slurry flow, which is divided into four categories. There are four types of flow: homogeneous flow, heterogeneous flow, moving bed flow, and stationary bed flow.

Homogenous flow

The fully suspended flow is the name for this type of flow. Finally, the solid particles are spread over the carrier fluid in this flow. Even at higher particle concentrations, most slurry flows are considered homogeneous when they contain high-velocity and fine particles. Because the particle concentration is uniform over the entire pipe cross section, the concentration and velocity profiles are in a vertical line. In [5] it is reported that drilling mud and clay are the two examples of evenly moving slurries, according to the report. Homogeneous flow is shown in Figure 2.

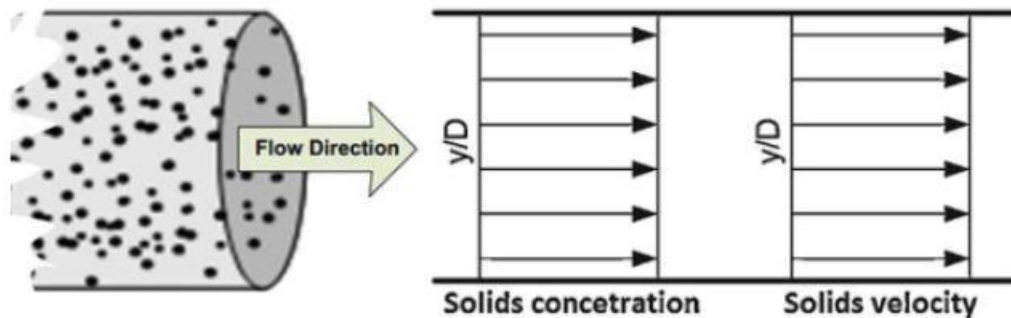


Figure 2 Homogenous flow [46]

Heterogenous flow

When the flow rate is reduced, probably particle separation occurs in the carrier fluid, resulting in a heterogeneous flow. Because solid particles do not mix evenly with carrier fluid, this pattern is a complicated flow regime. Fine particles will be in the top of the flow, whereas coarse and dense particles will be in the middle and bottom. The variation in particles suspended in the carrier liquid can be seen throughout the concentration distribution in the pipe cross section; however, there is no particle settling in the pipe. However, it should be emphasized that, in most cases, the heterogeneous flow has low solid concentrations. In [6] it is observed that the deposition velocities depend on the size, density of the particles, the concentration of solids, and the diameter of the pipe. Heterogeneous flow is shown in Figure 3.

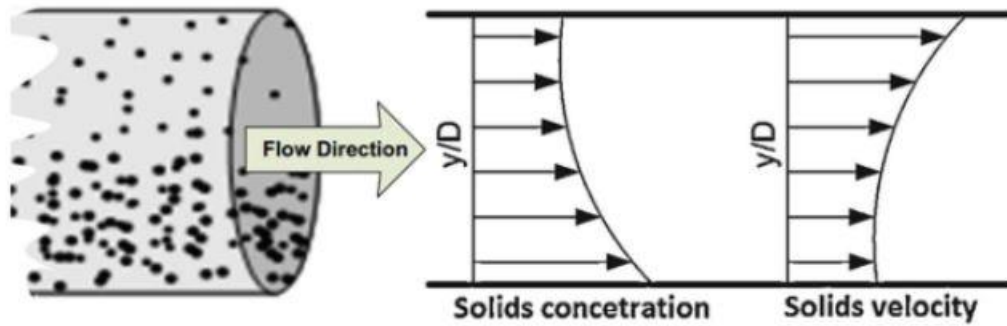


Figure 3 Heterogenous flow [46]

Moving bed flow

When the flow velocity falls below the heterogeneous velocity, a moving bed forms at the bottom of the pipe, which might cause resistance to wear. Because of this, coarse and dense particles form a flowing bed flow, with a larger concentration gradient at the bottom. Similarly, the velocity is low compared to the upper flow region. The upper layer of the bed flows faster than the lower layer because small particles are still suspended in the flow. The shear force of the carrier fluid is still strong enough to move this bed. In [7] it is found that moving the bed increases resistance to pipe wear. The flow of the moving bed is shown in Figure 4.

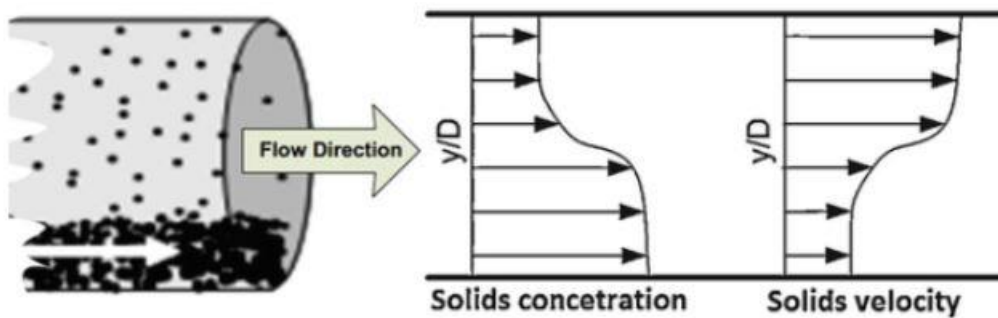


Figure 4 Moving bed flow [46]

Stationary bed flow

When the mean slurry velocity falls below that of the moving bed flow, it is impossible to move all the immersed particles, particularly those with the highest settling velocity (coarser and denser particles). As a result, they begin to settle and form a layer of the bed. Fine particles with low settling velocity, on the other hand are still suspended in the carrier fluid flow. The concentration of solid particles at the bottom is very high. A saltation flow is formed by solids moving over each other. In [7] it is reported that pipe blockage occurs in the flow on a stationary bed because it affects the pressure drop. The stationary bed flow is shown in Figure 5.

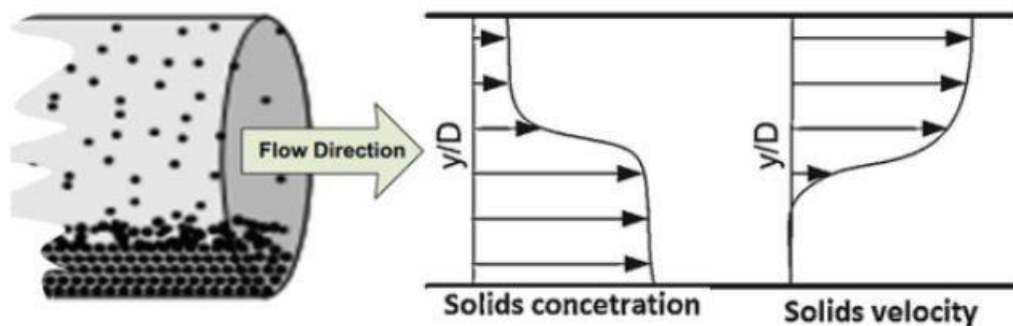


Figure 5 Stationary bed flow [46]

2. Measuring techniques of velocity and concentration profile

2.1. Laser Doppler Anemometry (LDA)

This method is used especially to determine the velocity of the flow. In [8] the LDA approach is carried out to identify the distributions of velocity and solid concentrations in a slow viscous slurry flow. The laser source is the most important factor in the LDA process and the results are also influenced by the laser source's energy. Initially, the laser source passes through a beam splitter by which the laser splits and passes through the transmitting lens then the laser strikes the test region, which aids in scattering the laser source as shown in Figure 6. When the source hits solid particles, it begins to emit in all directions. The incident frequency is not the same as the scattered frequency. The scattered frequency is proportional to the particle velocity; similarly, only the frequency that passes through the optics to the detector is seen and reported.

In [9] it is reported that the LDA technique is called point source measurement and as a result, no comprehensive velocity profile is obtained.

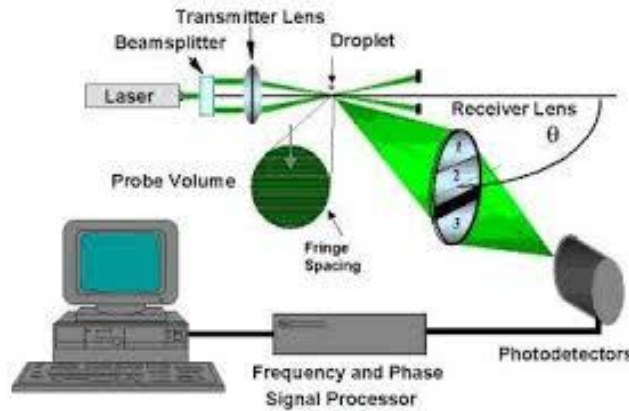


Figure 6 Laser Doppler Anemometry [48]

Application

- No calibration is needed
- Good spatial resolution

Limitation

- Multiple measurements are required to obtain the velocity profile, and it consumes more time
- Low solid fraction which must be 4%

2.2. Particle Image Velocimetry (PIV)

LDA is the foundation for the PIV approach. The entire velocity profile is produced using the PIV approach. The extra equipment that is employed, such as a CCD camera for collecting the flow patterns in frames per second. PIV operates by passing the laser pulse on a clear fluid flow along the seeding particles and the laser pulse is scattered by seeding particles. In [10] it is reported that the detector receives the scattered source from the seeding particles and the laser pulse should be kept constant during the time when the CCD camera captures photos of the sheet optics as shown in Figure 7. Seeding particles are sometimes known as tracers. The physical properties of the tracer must be identical to those of the solid particles in the flow. For proper data evaluation, the collected image should have a higher image density (mean number of images per unit of time) and the tracer particles in the image should also be higher. The acquired image is subjected to a cross-correlation approach (image comparison), and the images

mesh together at the same time. As a result, all options are summarized and a final meshing is created, from which the velocity profile is mapped. In [68] a digital masking technique is presented to separate the signals of a multiphase flow (two-phase).

Advantage

- High-speed data processing allows the generation of large numbers of image pairs
- The method is capable of measuring an entire two-dimensional cross section (geometry) of the flow field simultaneously

Limitation

- The discrete phase volume fraction should be less than 5% for better resolution and accuracy.
- Tracer particle is used

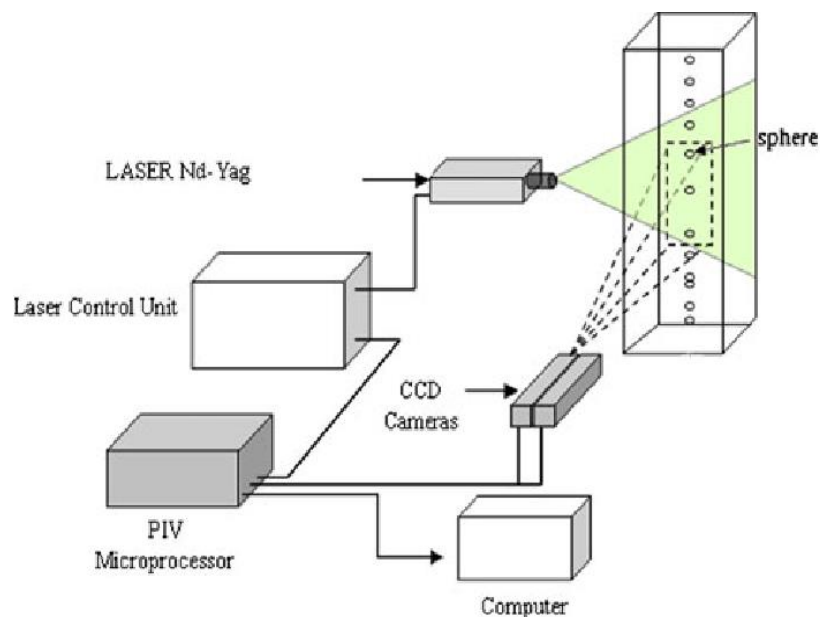


Figure 7 Particle Image Velocimetry [49]

2.3. Positron Emission Particle Tracking (PEPT)

The work [11] reported that the Positron Emission Particle Tracking is a method based on the tracking tracer particles and the emitted positrons. The study [12] stated that the PEPT technique relies on tracking a single neutrally buoyant tracer particle at a time and a closed-loop system is used, allowing the tracer seeding fluid to be recirculated. When this collided with an electron, it

produced a pair of back-to-back gamma rays, which are shown in Figure 8. Two detectors are also installed on either side of the flow. The detectors are only recorded if gamma rays are detected simultaneously by both detectors with resolving time. The PEPT camera is used to collect data and recreate the image in the future. In this scenario, a tracer is injected and circulated throughout the process, allowing for the mapping of a series of trajectories. The particles have recently been developed to be isokinetic with fluid. In basic geometry, the velocity profile of a Newtonian fluid flowing under laminar conditions can theoretically be calculated.

To reduce the load on the tracer particles, the fluid is circulated using a gear pump. It takes a long time for a single tracer particle to recirculate through the process. Additional tracer particles are injected in this scenario, which were always in the camera's field of view. This method does not require direct contact with the apparatus. The information collected by the camera restricts the number of velocity points that may be reliably recorded. The tracer particles are suspended along the flow, which does not disturb the flow regime. PEPT is used to calculate velocity, concentration, and flow pattern.

Advantage

- Complete velocity field measurement is possible
- Can be used in opaque system

Limitation

- The only way to get a better velocity profile is to use smaller tracer particles.
- It is challenging to design a tracer particle and to make it radioactive and is still in progress.
- It is quite costly and time-consuming.

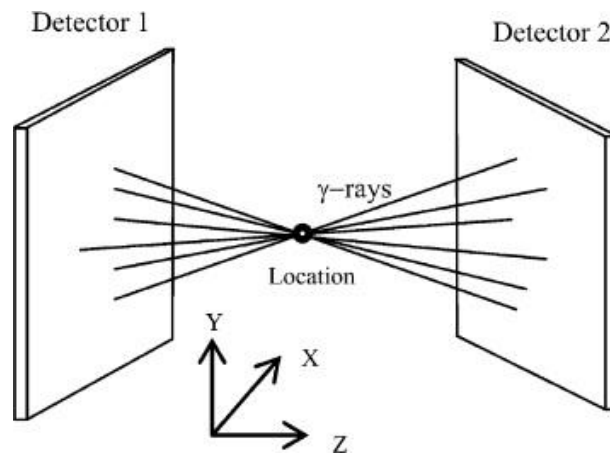


Figure 8 Positron Emission Particle Tracking [50]

2.4. Pulsed Ultrasonic Doppler Velocimetry (PUDV)

In [13] it is reported that PUDV technology uses doppler shift frequency and ultrasound waves through which the velocity and solid concentration profiles are calculated for fine particles. The Doppler change in the frequency of the ultrasonic signal dispersed by the streaming particles is used to determine velocity. When the number of particles that cross the measurement volume of the Doppler signal is compared with the number of particles that cross the control volume of the Doppler signal, the solid concentration can be calculated.

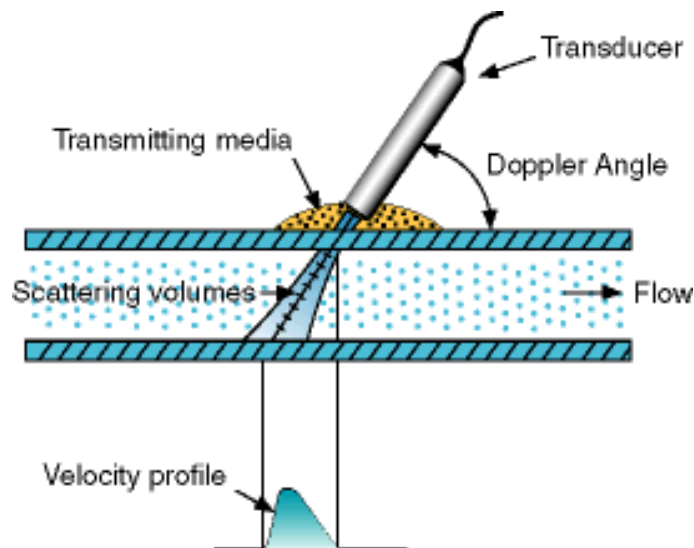


Figure 9 Pulsed Ultrasonic Doppler Velocimetry [51]

The piezo transducers emit a pulse of ultrasonic waves as it is shown in Figure 9. The scattered waves receive the emitted piezo, as the waves flow through the fluid and strike the particles with little or no attenuation. The experimental study [14] reported that plexiglass is used to decrease the ultrasonic reflection as it crossed the wall. Doppler, a data processor with an ultrasonic velocimeter, is used to process the signals. The information is saved in a digital oscilloscope. Software uses the frequency domain and the Fourier transform to process signals. For velocity measurement, the angle (Doppler angle) is critical (i.e., angle of the piezo transducer).

Advantage

- Velocity and concentration profiles of fine particles
- Flow information from a small portion of a vessel can be isolated and analyzed without interference from flow in adjacent areas

Limitation

- A higher concentration of solid cannot be penetrated.
- Travel distance is less and is not used for larger system.
- Low spatial resolution and average temporal resolution.

2.5. Gamma ray and X-ray tomography

Both techniques work on the same concept, with the only difference being the source of radiation. In the work [15] it is stated that the source is absorbed and some of it is attenuated as it passes through the flow medium and eventually reaches the detector. This approach is typically utilized for images of objects in steady state. The received data are transferred to the system, where they are rebuilt, and profiles are created. Compared to electrical tomography, this approach is relatively costly. The author of the work [16] used a multi-technique tomography method, combining electrical impedance tomography (EIT) with gamma ray for CFD (circulating fluidized beds), and found that the two techniques worked well together. The radiation produced by gamma rays is extremely high, so caution is advised. Some innovative solutions, such as fan beams, are being employed to reduce it. Radiation is stifled by a thick layer of lead. The authors of the work [45] measured the flow distribution across a distillation column using X-ray tomography on a packed bed column. The X-ray measuring apparatus is cumbersome, making field-sector measurements impossible. It is only possible for laboratory measurements, as shown in Figure 10.

Advantage and limitation

- Any flow can be measured
- Gamma ray radiation cannot be stopped, only blocked and safety precaution is high.
- The spatial resolution is high and the temporal resolution is low.

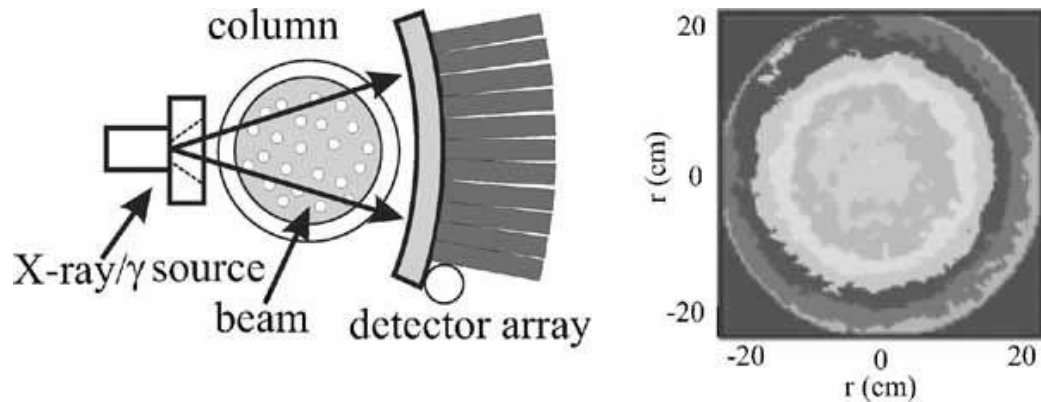


Figure 10 Gamma ray and X-Ray Tomography [52]

2.6. Electrical tomography technology

Electrical tomography is a special variant of tomography technology that is used in a variety of industrial settings. Low-frequency electromagnetic waves are used in this tomography to detect the passive electrical properties of the object, such as permeability, permittivity, and conductivity. This approach is noninvasive and inexpensive. Compared with advanced techniques such as MRI and X-ray, it is suitable for large-scale companies.

2.6.1. Electrical Impedance Tomography (EIT)

The concept is based on Ohm's law, which states that when a current is passed from a transmitting pair of electrodes into a conductive measuring object, the current induces a voltage differential on the remaining pair of electrodes as shown in Figure 11. In these electrode pair voltage difference measurements, the conductivity information is within the sensor zone. As a result, the measurement values can be utilized to estimate a process condition that is unknown. It is stated in the work [18] that the chemical process industries are the most common users of EIT. Because most substances are electrically conducting. The difference in electrical conductivity between the carrier fluid and the solid is significant (so EIT is used to determine the flow regime pattern).

Advantage and limitation

- It can be used for electrically conductive liquids and in chemical mixing and bubble column.
- The accuracy is not as good as in comparison to the ECT and ERT techniques.

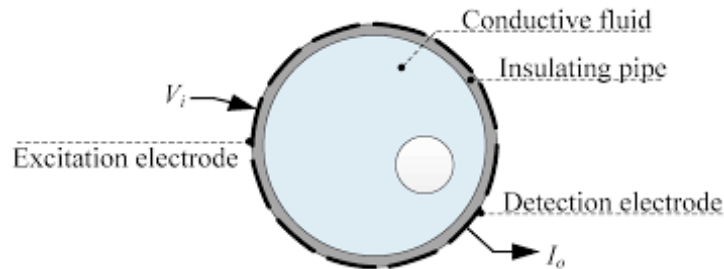


Figure 11 Electrical Impedance Tomography [53]

2.6.2. Electrical Capacitance Tomography (ECT)

The basic idea is to track the changes in capacitance produced by the distribution of the dielectric material. ECT refers to imaging techniques that contain dielectric materials, as shown in Figure 12. In the work [19] it is stated that the distribution of image permittivity for low or optimal non-conducting materials is the goal of ECT.

Capacitance is a property of the sensor. In the work [20] it is stated that the capacitances were measured using a series of electrode sensors located around the perimeter of the pipe. ECT uses a sinusoidal voltage as it is sending signal. Electric charges are established in the remaining pair of electrodes, reflecting the permittivity distribution of the measuring material. A cross-sectional image is created and used to reconstruct the capacitance measurements using an algorithm. The authors of the work [21] that the ECT is a soft field approach, the reconstruction of pictures is complex due to the non-linear relationship between permittivity and capacitance measurement distribution. ECT electrodes do not have to be in contact with the object being measured.

Advantages and limitations

- Target- dielectric materials (gas, oil, nonmetallic powders, polymers)
- Mineral transportation, fluidized bed, oil and gas flow and pharmaceutical process.
- Poor spatial resolution compared to radioactive methods (Gamma and PEPT). To improve this artificial neuron network are used.

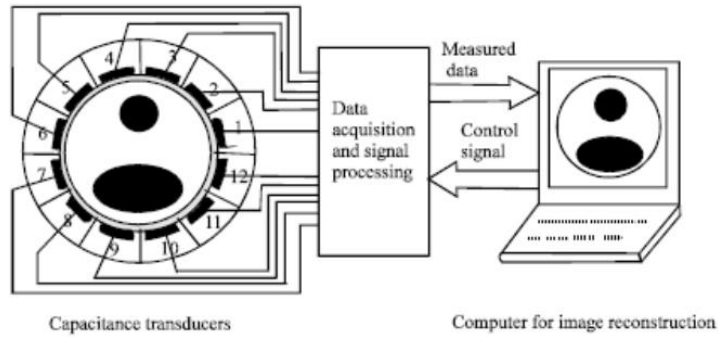


Figure 12 Electrical Capacitance Tomography [54]

2.6.3. Electro Magnetic Tomography (EMT)

Magnetic induction tomography and eddy current tomography are other names for it. In [17] the principle is based on the measurement of mutual inductance. Due to the primary magnetic field, a potential is created on the receiving coil by injecting a sinusoidal current into the magnetic coil. Sensitivity is assessed when the excitation frequency is increased. A secondary magnetic field is created when an object is placed between the transmitting and receiving coils. The receiving coil will then pick it up. The conductivity distribution in the region between the receiving and transmitting coils determines the induced voltage. Although electrical conductivity and permeability tomography may be reconstructed, the focus is primarily on conductivity. EMT is frequently used to replace EIT. Because EMT is also affected by conductivity. The magnetic field and the detection coil are shown in Figure 13.

Advantage and limitation

- Target - electrically conductive materials (water/saline, metals, minerals, magnetic materials).
- Molten metal flow, two-phase flow, bubble columns and non-destructive testing
- The best suitable for flow rate measurement and is not highly preferred method for velocity and concentration profile measurement.

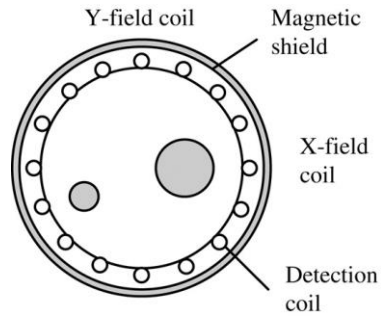


Figure 13 Electric Magnetic Tomography [55]

2.6.4. Electrical Resistance Tomography (ERT)

The technique involves visualizing mixes in a pipe or vessel without physically seeing them inside the system and it has drawn the attention of many researchers and industry because of its safety and low cost. In [22] it is reported that the purpose of the ERT is to determine the resistance distribution in a given domain. The continuous phase (carrier fluid) is conductive, but the scattered phase (solid) is less conductive. ERT uses electrical resistance measurement and image reconstruction to create a 2D or 3D image. ERT techniques include the sensor with electron rings, the DAS system, the image reconstruction system, and the host computer from which the image is formed. The ERT approach is used to observe the flow of the slurry by placing the electrode on the periphery of the tube wall, as shown in Figure 14. Because of the quick electrical measurement, it offers a sensing technique with good time resolution. ERT, on the other hand, injects low electrical current through a pair of adjacent electrode borders and measures the potential difference between the remaining electrodes. To achieve full rotation, the same technique is repeated up to the last pair of electrodes, resulting in a collection of data. In [23] it is stated that by using the adjacent technique, it is implemented for 104 independent differential voltage measurements using a most common dual plane configuration electrode setup to obtain accurate values. In [24] the dual-plane ERT has the ability to be used in a variety of additional multiphase applications where the flowing components have a large variation in conductivity and the continuous component is not an electrical insulator.

Concentration tomography is the process of interpreting each data sheet provided by an image reconstruction technique to obtain a cross-sectional image that corresponds to the electrical conductivity filled within the pipe. In [25] it is reported that the linear back projection is used to recreate the image. Due to their fast electrical measurements, electrical resistance tomography

detection has exceptional time resolution. This, according to aids in determining a minimal particle size with spatial resolution.

Advantages

- High temporal resolution and low-cost and non-radiation emitting.
- Used in mining, chemical and mixing.
- High speed and high precision are possible with neural networks

Limitations

- Need to increase sensor spatial resolution
- Development of more accurate image reconstruction, as inaccurate images will interpret inaccurate flow parameters, such as volume flow rate.
- Improvement of design both mechanically and electrically

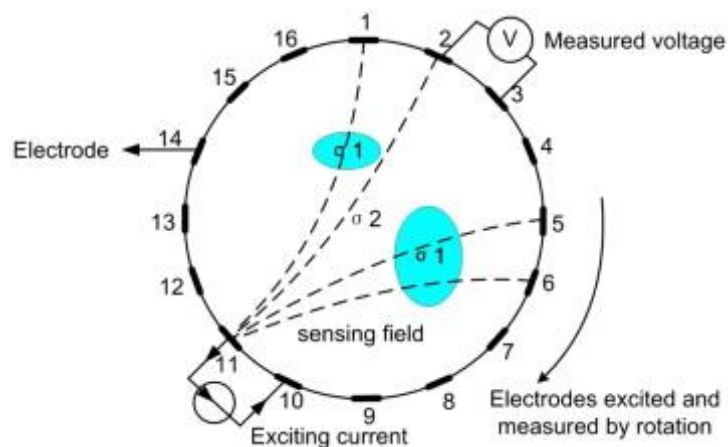


Figure 14 Electrical Resistance Tomography [56]

2.7. Magnetic Resonance Imaging (MRI)

When a burst of radio frequency hits an object subjected to a magnetic field, its hydrogen protons spin randomly and line up in the direction of the magnetic field, and they flip around. In [26] the author stated that when the protons return to their original position and send a radio signal in the form of an echo, which is known as nuclear magnetic resonance. The hydrogen protons react by releasing an electromagnetic signal. The signal is received as a radio frequency by the scanner, which is then used to build a high-resolution image of the flow. A tiny magnetic field is used to treat hydrogen atoms. In [27] magnetic resonance imaging can be used to

determine the volume fraction, physical behavior, and physical properties of multiphase. Inline measurement is possible in a full-bore configuration without the need for a radiation source. Any other source of principle measurement is irrelevant. The velocity and concentration profiles are calculated using the RF frequency. Compared to other techniques, the spatial and temporal resolution is great. In [27] it is reported that MRI is a specialist technology that cannot be used in today's business since it is not suitable for all materials because the object must have at least one carbon or hydrogen atom, and the test section must be smaller than the magnetic field (size) as shown in Figure 15.

Advantage

- High spatial and temporal resolution.
- No radiation-based technique.

Limitation

- A high magnetic field is required.
- Cannot be used for all material forms and is still under development.

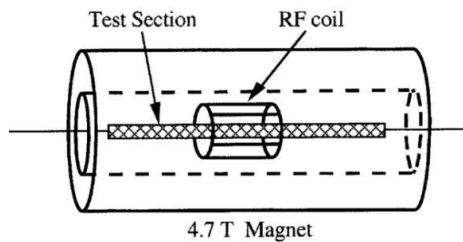


Figure 15 Magnetic Resonance Tomography [57]

3. Temperature Profile Measurement Techniques

Thermocouple, thermistor, thermowell, infrared thermography, liquid crystals, particle image thermography, temperature-sensitive paints, laser-induced fluorescence, and magnetic resonance thermography are common temperature measurement techniques. However, because the thermocouple, thermistor, and thermowell are point sources of measurement, obtaining a temperature profile takes time.

3.1. Thermochromic Liquid Crystals (TLC)

Thermochromic liquid crystals work on the same principle of particle image velocimetry. In [28] reported that the thermochromic liquid crystals and seeding particles are used in digital

particle image thermometry DPIT. During the cross section of the flow is illuminated by a collimated source of white light and the color pictures are acquired perpendicular to the stream. The temperature is determined by examining the reflected wavelength of the seeding particles. The captured images by the CCC RGB cameras can be calibrated for the color temperature response and analyzing the images with appropriate image processing software. The most common method is micro-encapsulation, in which liquid crystals are covered with polymer and are as small as micrometers. When liquid crystals disperse in a liquid, they act as both a tracer particle and a tiny thermometer for monitoring fluid temperature.

Advantage

- It is flexible to use from micron-sized to micrometer sized.
- High spatial resolution

Limitation

- Point source of measurement and it consumes long time for full measurement field

3.2. Infrared Thermography (IRT)

Infrared thermography is used to measure the temperature of the particles. Solid particles emit IR rays from the surface of the particles and the emitted rays are detected by a camera. Therefore, the infrared energy is proportional to the surface temperature of the solid particle. The temperature of objects or solid particles can be measured by measuring the infrared energy. The polished solid tracer particles are not used because of the reflection. In [29] the solid particles are coated with black to avoid multiple reflections. Multiple reflection results are difficult to evaluate for temperature measurement. It shows how a fully computerized infrared imaging system meets both quantitative and qualitative requirements.

Application

- It is a non-contact and non-destructive test method, used from a safe distance
- IR cameras are relatively easy to use

Limitation

- Obtaining high accuracy can be difficult due to varying emissivity of the different materials.

- It is necessary to have a direct view of the electrical components being scanned; covers must be removed, which can be a hazardous activity.

3.3. Magnetic Resonance Thermometry (MRT)

The MRT principle is based on magnetic resonance imaging (MRI). To validate the data and better define the heat transport properties of the system, magnetic resonance spectroscopy (MRT) is frequently used in conjunction with MRC or MRV. In [30] the author used MRT to measure 2D and 3D temperature fields at millimeter resolution. Later, MRV-MRT is used to generate 3D temperature and velocity profiles of straight-pipe flows at various flow rates. Similarly, MRT and MRC used to investigate a hot jet in crossflow and temperature measurement had a $\pm 1^\circ\text{C}$ uncertainty, making it the most precise MRT measurement to date. However, when the temperature of the heated jet exceeded the glass transition temperature of the water channel, everyone experienced material failure problems.

Application

- Applicable for turbulent and complex flow.
- Full field of temperature measurements unlike measurement probes

Limitation

- Not suitable for outside-environment measurement, it is only meant for lab measurements
- The testing area should not be higher than the magnetic zone.

3.4. Laser Induced Fluorescence (LIF)

Laser-induced fluorescence (LIF) or laser-stimulated fluorescence (LSF) is a spectroscopic technique in which an atom or molecule is driven to a higher energy level by absorbing laser light and then emitting the light spontaneously. In [31] the LIF technique measures passive scalars, such as temperature and concentration. It is also known for non-intrusive techniques. In [69] this technique is applied to detect the mixing surface employed by LIF for the measurement of temperature and velocity fields. Fluorescence intensity also depends on temperature. However, this technique is a point source of measurement and similarly, it is an expensive method.

Application

- LIF can be combined with particle image velocimetry and it allows for the simultaneous measurement of a fluid velocity field and species concentration

Limitation

- signal-to-noise ratio often limited by detector shot-noise ratio
- temperature measurements typically require two laser sources

Chapter II – Calculation of limiting suspension parameters

The aim of this chapter is to describe the calculation of a low-concentrated suspension of fine particles and a high-concentrated suspension of coarse particles. These two different concentrated particles have different velocity, flow rate, density and settling region. Based on this calculation we can limit the minimum and maximum dimensions for piping size, pump proposal, heating units, etc. The below-mentioned calculated values are for the particles of 10 microns and this was considered as a reference for re-calculating to particles for 2 microns.

1. Low concentrated suspension of fine particles of 10 microns with 5 V/V% solid concentration

Density of water ρ_l	998 kg/m ³
Density of glass beads ρ_g	2467 kg/m ³
Diameter of glass bead d_p	0.00001m
Viscosity of water μ_l	0.001005 Pa.s
Volume fraction of slurry C_v	0.05
Gravity constant g	9.81 m/s ²

In [32] the density of fluid phase effectively becomes the bulk density of slurry ρ_m which follows as:

$$\rho_m = C_v \rho_g + (1 - C_v)\rho_l \quad (2.2)$$

Substituting the variables C_v, ρ_g, ρ_l in eq (2.1)

$$\rho_m = 1071.45 \text{ kg/m}^3$$

In [32] the empirical correlation ψ_p

$$\psi_p = \frac{1}{10^{1.82(1-C_v)}} \quad (2.2)$$

$$\psi_p = 0.01866$$

The velocity and settling region of the glass beads suspended in water should be calculated. We need to decide in which region the particles settle in the water. For that we have a number. It is called $C_D Re^2$.

$$C_D Re^2 = \frac{4 g d_p^2 (\rho_g - \rho_l)}{3 \mu_l^2} \quad (2.3)$$

For Stoke's region $C_D Re^2 < 48$

$$C_D Re^2 = 0.01898 \text{ lies in Stokes's region}$$

In the Stokes region velocity (v_t) of laminar settling will be based on density and diameter of particles but for future we need to consider the concentration of particles to achieve proper deposition velocity.

$$v_t = \frac{g d_p^2 (\rho_g - \rho_l)}{18 \mu_l} \quad (2.4)$$

Substituting the variables $g, d_p, \rho_g, \rho_l, \mu_l$ in eq (2.4)

$$v_t = 7.97 e^{-05} \text{ m/s}$$

In [32] the viscosity of slurry μ_m is based on viscosity of liquid and empirical correlation

$$\mu_m = \frac{\mu_l}{\psi_p} \quad (2.5)$$

$$\mu_m = 0.05385 \text{ Pa.s}$$

In [32] the Reynold's number calculated to identify the flow regime or region, when Re is less than 1 it lies in the Stoke region.

$$Re = \frac{d_p v_t \rho_m}{\mu_l C_v} \quad (2.6)$$

$$Re = 1.70 e^{-02} \text{ (lies in Stokes's region)}$$

1.1. Calculation of velocity

Considering steel tube as 60.3 x 2 mm. $D_1 = 56.3 \text{ mm}$

It is important to calculate the terminal deposition velocity V_D for given volume fraction C_v , because to know at what velocity the particle settles. In [33] it is derived as a correlation that describes the behavior of concentration slurries (up to 40%)

$$V_D = 4.0 (d_p/D_1)^{\frac{1}{6}} (C_v)^{\frac{1}{5}} \sqrt{2gD_1 \left(\frac{\rho_l}{\rho_g} - 1 \right)} \quad (2.7)$$

Substituting the variables $d_p, D_1, C_v, g, \rho_l, \rho_g$ in eq (2.7)

$$V_D = 6.64e^{-01} \text{m/s}$$

In [26] it is reported that the operating velocity in settling the slurry transport in horizontal pipes should be 1.3 times higher than the terminal deposition velocity V_D

$$V_D = 0.8635 \text{ m/s}$$

The volumetric flow rate depends on the area of the pipe and the velocity of the flow,

$$Q_v = A_1 \times V_D \quad (2.8)$$

Area of the tube,

$$A_1 = \frac{\pi}{4} D_1^2 \quad (2.9)$$

From eq (2.9) for the diameter of the tube D_1 we can find the area A_1 is 0.002489 m^2 and substituting the variables A_1, V_D in eq (2.8) the volumetric flow rate is obtained Q_v is $0.00215 \text{ m}^3/\text{s}$

1.2. Mixing tank calculation

Considering the volume of slurry V as 100 liters, it is enough for suspension to fill the entire piping system in the experimental layout. So, the total volume of slurry V is 0.1 m^3

Let's assume internal Diameter of tank D_{in} is 0.496 m

Tori spherical part – Type E

Even while flat bottom tanks are ubiquitous and save shaft length, they do not drain very well, especially when solids or high viscosity fluids are present. Torispherical or dished bottoms, on the other hand, provide good strength, axial flow patterns and drainage performance.

In [34] from the catalogue volume of the torispherical V_t is 0.015 m^3

Height of the torispherical H_t is 0.112 m

Cylindrical part

Height of the cylindrical shell need to be calculated based on tank diameter

Volume of cylinder without dished end (V_c) = $0.1 - 0.015$

$$V_c = 0.085 \text{ m}^3$$

$$H_c = \frac{4 V_c}{\pi D_{in}^2} \quad (2.10)$$

Substituting the variables V_c, D_{in} in eq (2.10) the cylindrical height H_c is 0.4399 m

Total height of slurry in mixing tank $H = H_c + H_t$

$$H = 0.552 \text{ m}$$

The slurry level rises because the agitator, baffle, and shaft all take up a certain amount of area inside the mixing tank. As a result of the mixing tank height can be considered as, $H = 0.7 \text{ m}$

1.3. Pressure calculation

Atmospheric pressure at surface of mixing tank $P_{atm} = 101325 \text{ Pa}$

Pressure at bottom of tank P_b

$$P_b = \rho_m g H + P_{atm} \quad (2.11)$$

$$P_b = 5801.104 + 101325$$

$$P_b = 107126.104 \text{ Pa}$$

2. High concentrated suspension of coarse particles 2 mm with 30 V/V % of Solid concentration

The calculation procedure for high concentrated suspension of coarse particles 2 mm glass beads follows similar procedure to the low-concentrated suspension of fine particles with 10 microns. By which the bulk density of slurry ρ_m is 1438.70 kg/m³ and the settling region $C_D Re^2$ is $1.52 e^{05}$ lies in the Newton's region ($48 < C_D Re^2 < 1.1 \times 10^5$). It is noticed that two different sized glass bead particles settle in two different regions.

For Newton's region the velocity v_t for 2 mm particles,

$$v_t = 1.74 \sqrt{\frac{d_p g (\rho_g - \rho_l)}{\rho_l}} \quad (2.12)$$
$$v_t = 2.96 e^{-01} \text{ m/s}$$

Similarly, for calculating other variables of 2 mm particles, the same method is followed as a low concentrated suspension of fine particles with 10 microns. The Reynolds number Re is 2822 lies in Newton's region ($500 < Re < 3 \times 10^5$), the terminal deposition velocity V_D is 2.988 m/s, the volumetric flow rate Q_v is 0.00744 m³/s and the pressure at bottom of tank P_b is 109114.489 Pa.

Chapter III – Gravitational Method

1. Gravitational flow

Gravitational flow for water distribution does not require any external power and it is more reliable and cost-effective than pumping fluids. To avoid using external power, one method in this experiment uses the gravitational flow principle.

1.1. Frictional losses

There are two categories of losses: significant losses and minor losses. The frictional interaction between the pipe wall and the moving fluid causes significant losses. Minor losses occur when there is a disruption in the flow, which might be caused by fittings or valves and the values for frictional losses are in shown in Table 1. In most cases, these losses are insignificant.

Table 1 Frictional losses for valves and fittings [32]

Types of Fittings & Valve	Frictional loss, K_f
Elbow 90°	0.95
Diaphragm valve	2.3
Tee	1.45
Reducer	0.5
Expander	0.25

In [32] the contraction loss at exit from mixing tank

$$e_z = 0.55 \left(1 - \frac{A_1}{A_m}\right) \frac{V_D^2}{2 \alpha} \quad (3.1)$$

$$\text{Area of tank } A_m = 0.19322 \text{ m}^2$$

$$Re = \frac{\rho_m V_D D_1}{\mu_m} \quad (3.2)$$

$$Re = 967.99 \text{ (lies in laminar flow)}$$

In [32] the α is 0.5 for laminar flow. The contraction frictional loss at mixing tank e_z is 0.4048 J/kg

In [32] the friction loss in length tube

$$e_z = 4 f \frac{\Delta L}{D_1} \frac{V_D^2}{2} \quad (3.3)$$

Fanning friction factor f

$$f = \frac{16}{Re} \quad (3.4)$$

From eq (3.4) by substituting the variable Re , the fanning friction factor f is 0.016

$\Delta L = 13.315$ m (Overall length of the pipe ΔL is basically estimated from a simple experimental layout and in our experimental stand we are also using clear tubes for the test section). The frictional loss for the overall length of the tube e_z is 5.833 J/kg from eq (3.3).

In [32] the loss in elbows – 5 pcs

$$e_z = K_f \frac{V_D^2}{2} \quad (3.5)$$

From (Table 1) for elbow K_f is 0.95 by substituting the variables K_f, V_D in eq (3.5). The friction loss for elbow e_z is 1.7708 J/kg

In [32] the loss by diaphragm valves in DN 50 pipe - 2 pcs

From (Table 1) for diaphragm valves K_f is 2.3 by substituting the variables K_f, V_D in eq (3.5). The friction loss for diaphragm valve e_z is 1.715 J/kg

In [32] the sudden expansion loss at inlet of storage tank

$$e_z = \left[1 - \frac{A_1}{A_m} \right]^2 \frac{V_D^2}{2 \alpha} \quad (3.6)$$

During sudden expansion loss at the entry of storage tank e_z is 0.727 J/kg

Total frictional loss $\sum e_z = 10.45$ J/kg (Sum of all losses). On the basis of total frictional loss, the pressure drop over the length of the pipe can be determined along with slurry density.

$$e_z = \frac{\Delta P_z}{\rho_m}$$

The pressure drop ΔP_z for the total frictional loss is 11197.39 Pa.

Based on the same calculation procedure for the 2 mm particle, the Reynolds number Re is 12814 lies in turbulent flow and hence α is considered as 1. So, for this condition, it is necessary to calculate only the friction loss in pipe and other losses are followed the same as for low concentrated particle 10 microns. For the frictional loss in the pipe, the friction factor λ which depends on the relative roughness k^* of the pipe and Reynolds number Re . Therefore, the tube is considered as a new pipe as a seamless steel-drawn pipe. In [32] it is reported that for new seamless steel-drawn pipe the absolute roughness k_{av} is 0.04 mm.

The relative roughness of the pipe

$$k^* = \frac{k_{av}}{D_1} \quad (3.7)$$

Substituting the variables k_{av}, D_1 in eq (3.7) the relative roughness of the pipe k^* is $7.1 e^{-04}$

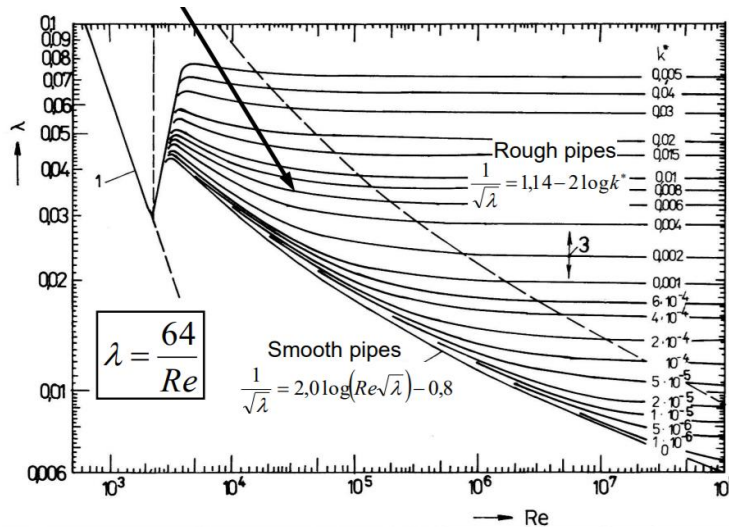


Figure 16 Friction factor graph [32]

The friction factor can be calculated from Figure 16 based on the dependence of the Reynolds number Re 12814 and the relative roughness of the pipe $k^* = 7.1 e^{-04}$. Therefore, the friction factor λ is 0.03.

$$e_z = \lambda \frac{\Delta L}{D_1} \frac{V_D^2}{2} \quad (3.8)$$

The frictional loss in the pipe can be calculated by substituting the parameters $\lambda, \Delta L, V_D$ in eq (3.8). Therefore V_D is 2.988 m/s terminal deposition velocity of 2 mm particles and ΔL remains

same as 13.315 m. The frictional loss in pipe e_z is 31.675 J/kg and the total frictional loss $\sum e_z$ is 82.62 J/kg and pressure drop ΔP_z is 118858.33 Pa

1.2. Mixing tank height from bottom

To estimate the height at which the mixing tank should be located to produce the appropriate velocity V_D for fine particles, it is necessary to calculate h_1 and h_2 is datum point. We can determine the required height using the Bernoulli energy equation and accounting for all losses h_1 and datum point $h_2 = 0$ as shown in Figure 17.

P_1 and P_2 are at atmospheric pressure and $V_1 = 0$ (at initial point there is no velocity)

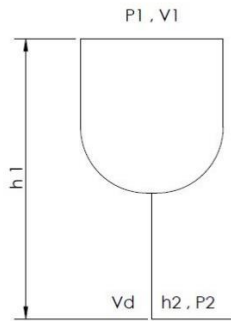


Figure 17 Mixing tank height

$$\frac{V_1^2}{2} + \frac{P_1}{\rho_m} + gh_1 = \frac{V_D^2}{2} + \frac{P_2}{\rho_m} + gh_2 + \sum e_z \quad (3.9)$$

Substituting the variables P_1 & P_2 , $\sum e_z$, V_1 & V_D , h_2 in eq (3.9)

$$gh_1 = \frac{1}{2} V_D^2 + e_z$$

The required height to achieve the velocity V_D for fine particles, h_1 is 1.103 m

Based on the same calculation procedure for 2 mm particles h_1 is 8.876 m

1.3. Pump calculation

Although we set up the experimental loop with gravitational flow, it is necessary to return the slurry to the experimental loop from the storage tank to the mixing tank by the pump. The power necessary to return the slurry should be calculated and friction losses in pipe fittings and valves

should also be considered. When returning, the flow rate can be increased higher than the terminal deposition velocity and it can be considered as m_s is 5 kg/s with a velocity V_D of 1.875 m/s and Reynolds number Re is 2100.

1.3.1. Frictional losses in pipe, fittings, and valves

During the pump calculation, both minor and severe losses should be considered. Therefore, it is necessary to calculate all the losses.

Contraction loss at exit from storage tank

The contraction loss at exit from the storage tank can be calculated from Eq. (3.1) by substituting the variables A_1, A_m, V_D . Since, Re is 2100 it lies in transition flow and α is considered as 1. Therefore, the contraction loss e_z is 0.9538 J/kg

Loss in elbows – 3 pcs

From (Table 1) for elbow K_f is 0.95 by substituting the variables K_f, V_D in eq (3.5). The friction loss for elbow e_z is 5.007 J/kg

Loss by Diaphragm valves – 1 pc

From (Table 1) for diaphragm valves K_f is 2.3 by substituting the variables K_f, V_D in eq (3.5). The friction loss for diaphragm valve e_z is 4.041 J/kg

Friction loss in length tube

$\Delta L = 2.5$ m (initially the overall length of the pipe to return the slurry from the storage tank to the mixing tank is 1.39 m and it is necessary to consider h_1)

In Figure 16 on the dependence of Reynolds number Re is 2100 and the relative roughness of the pipe k^* is $7.1 e^{-04}$ The friction factor λ is 0.04 and substituting the parameters in eq (3.8). The frictional loss in pipe e_z is 3.11/kg and the total frictional loss $\sum e_z = 13.840$ J/kg and pressure drop ΔP_z is 14829.784 Pa.

Based on the same calculation procedure, the total frictional loss for 2 mm particles $\sum e_z$ is 178.40 J/kg and pressure drop ΔP_z is 256667.36 Pa

1.4. Pump power

The velocity is neglected because the volumetric flow rate is same $v_2^2 - v_1^2 = 0$

The atmospheric at both sides is neglected $P_2 - P_1$ is 0 and the static height between the mixing

tank and storage tank h_2 is 1.844 m and h_1 is datum point.

In [32] we can obtain the mechanical shaft work as

$$\frac{1}{2\alpha}(v_2^2 - v_1^2) + g(h_2 - h_1) + \frac{P_2 - P_1}{\rho_m} + \sum e_z + W_s = 0 \quad (3.10)$$

Substituting all the values in eq (3.10), mechanical work delivered to fluid per mass of fluid W_s ,

$$-W_s = 31.93 \text{ J/kg}$$

So, the mechanical work delivered to fluid per mass of fluid W_s results in negative. It shows that the pump needs to provide work to the system.

Mechanical pump work W_p ,

$$-W_s = \eta W_p \quad (3.11)$$

Assume pump efficiency $\eta = 70 \%$

$$W_p = 45.61 \text{ J/kg}$$

The pump power P is calculated based on the mass flow rate of slurry m_s and mechanical pump work W_p

$$P = m_s W_p \quad (3.12)$$

Mass flow rate m_s considered approximately twice the amount of flow rate obtained during the gravitational flow.

$$m_s = 5 \text{ kg/s}$$

Substituting the variables m_s, W_p in eq (3.12) the required pump power P is 0.228 kW

Based on the same calculation procedure for 2 mm particle the required pump power P is 7.87 kW.

1.5. Net positive suction head (NPSH)

The available net positive suction is calculated based on the relation between the pressure on the pump suction side to the density of the slurry by gravitational flow,

$$NPSH_a = \frac{P_s}{\rho_m g} \quad (3.12)$$

The vapor pressure P_{vp} at this point it depend on the working temperature 80°C and the vapor pressure (from steam table for 80 °C) P_{vp} is 47.36 kPa. The static head h_{sh} is the height difference between the slurry surface of the storage tank and the pump inlet. We can consider the storage tank of the slurry surface for the maximum height H is 552 mm and the height between the storage tank bottom and the pump inlet is 433 mm. So, the static head h_{sh} is 985 mm. Towards the suction side, it is necessary to calculate the frictional losses. On the suction side the total length of the pipe is 927 mm and the friction loss is calculated from eq (3.8). Therefore, the frictional loss in pipe is e_z is 1.16 J/kg. The other two parameters are one diaphragm valve the frictional loss e_z is 4.04 J/kg from eq (3.5) and one elbow the frictional loss e_z is 1.67 J/kg from eq (3.5). The total frictional loss at suction side e_{zs} is 6.87 J/kg. Let assume P_1 as atmospheric pressure the slurry surface of the storage tank. Velocity of the flow V_D is 1.875 m/s since we are pumping the slurry from the storage tank to the mixing tank, the velocity is assumed approximately twice the deposition velocity.

$$P_s = \frac{\rho_m V_D^2}{2} + P_1 + \rho_m g h_{sh} - \rho_m e_{zs} - P_{vp} \quad (3.13)$$

Substituting the variables $\rho_m, P_1, e_{zs}, P_{vp}, V_D$ in eq (3.13) the pressure at suction side P_s is 58842.92 Pa.

The net positive suction side can be calculated by substituting the variables P_s, ρ_m, g in eq (3.12) the available $NPSH_a$ is 5.59 m.

Based on the same calculation procedure for coarse particles 2 mm the pressure at suction side P_s is 6317.47 Pa and the available $NPSH_a$ is 0.447 m.

Chapter IV – Pumping Method

1. Pumping flow

Instead of using gravity to transport the fluid, a pump is used. It is simple to control the flow of the slurry with a pump, and the pumping requires external power. As a result, the required pump power must be estimated.

1.1. Frictional losses in pipe, fittings, and valves

Some large and minor losses may occur during pipe flow and this should be reported similarly to the gravitational technique. For fine particles the terminal deposition velocity V_D is 0.8635 m/s, the diameter of tube D_1 is 56.3 mm and the geometry dimensions of tank are considered the same as the gravitational flow and therefore the Reynolds number also lies in the laminar flow as density of slurry ρ_m is 1071.45 kg/m³ and viscosity of slurry μ_m is 0.05385 Pa. s.

Contraction loss at exit from mixing tank

The contraction frictional loss at mixing tank e_z is 0.405 J/kg same as gravitational flow.

Friction loss in length tube

$\Delta L = 13.315\text{m}$ (overall length of pipe from experimental layout)

From eq (3.3) substituting the variables ΔL , Re , f . The frictional loss for the overall length of the tube e_z is 5.834 J/kg.

Loss in elbows 6 pcs

From (Table 1) for elbow K_f is 0.95 by substituting the variables K_f , V_D in eq (3.5). The friction loss for elbow e_z is 2.125 J/kg

Loss by Diaphragm valves 2 pcs

From (Table 1) for diaphragm valves K_f is 2.3 by substituting the variables K_f , V_D in eq (3.5). The friction loss for diaphragm valves e_z is 1.715 J/kg

Sudden expansion loss at storage tank entry

From eq (3.6) by substituting the variables A_m, A_1, V_D . The sudden expansion loss at the entry of storage tank e_z is 0.727 J/kg same as gravitational flow.

Loss by reducer

From (Table 1) for reducer K_f is 0.5 by substituting the variables K_f, V_D in eq (3.5). The friction loss for reducer e_z is 0.186 J/kg.

Loss by expander

From (Table 1) for expander K_f is 0.25 by substituting the variables K_f, V_D in eq (3.5). The friction loss for expander e_z is 0.093 J/kg.

Hence, the total frictional loss $\sum e_z$ is 11.084 J/kg (Sum of all losses). Based on the total frictional loss, the pressure drop through the length of the pipe can be determined along with the slurry density. So, the pressure drop ΔP_z is 11876.46 Pa

Based on the same calculation procedure for 2 mm particle the total frictional loss $\sum e_z$ is 87.78 J/kg and pressure drop ΔP_z is 126290.24 Pa

1.2. Pump power

An external power supply is required to run a pump. The useful power transmitted to the fluid treated by the pump is known as the output power.

Velocity is neglected because volumetric flow rate is same at mixing tank and storage tank

$$\text{surface } V_2^2 - V_1^2 = 0$$

Atmospheric pressure at mixing tank and storage tank surface is neglected $P_2 - P_1 = 0$

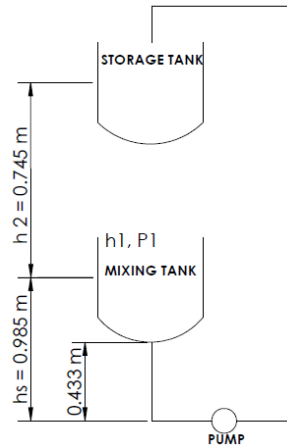


Figure 18 Simple pumping circuit

The static height between the mixing tank and storage tank h_2 is 0.745 m and we can consider h_1 as datum point as shown in Figure 18.

Substituting all the values in eq (3.10), We can obtain, work delivered to fluid per mass of fluid W_s

$$-W_s = 18.39 \text{ J/kg}$$

Mechanical pump work W_p ,

$$-W_s = \eta W_p$$

Assume efficiency $\eta = 70 \%$

$$W_p = 26.275 \text{ J/kg}$$

Pump power P calculated based on mass flow rate of slurry m_s and mechanical pump work W_p

$$P = m_s W_p$$

Mass flow rate m_s is determined by volumetric flow rate Q_v is $0.00215 \text{ m}^3/\text{s}$ and density of slurry ρ_m

$$m_s = Q_v \rho_m$$

$$m_s = 2.303 \text{ kg/s}$$

The required pump power P is 0.061 kW and the electric power input P_e is 0.086 kW the pump power P divided by efficiency η

Based on the same calculation procedure 2 mm particles the required pump power P is 1.45 kW and the electric power P_e is 2.07 kW.

The pressure developed at discharge end of the pump can be calculated based on Bernoulli's energy equation from eq (3.9), relation between the pump discharge point 1 and storage tank surface point 2. Pressure at surface of storage tank is P_2 is 101325 Pa.

$$P_1 = \left(\frac{P_2}{\rho_m} + gh_2 + e_z - \frac{V_D^2}{2} \right) \rho_m \quad (4.0)$$

$$P_1 = 125415.12 \text{ Pa}$$

Based on the same calculation procedure 2 mm particles $P_1 = 247951.76 \text{ Pa}$

1.3. Calculation of minimum speed of impeller (N_{js})

Internal diameter of mixing tank $D_{in} = 0.496 \text{ m}$

Height of tank $H = 0.7 \text{ m}$

Diameter of particle for low concentrated suspension fine particle d_p is 10 microns

Diameter of pitch blade agitator $D_a = \frac{D_{in}}{3} = 0.165 \text{ m}$

Concentration by weight of solids in a mixture is expressed as:

$$C_w = C_v \rho_g \frac{1}{\rho_m} \quad (4.1)$$

$$C_w = 0.12$$

In [35] the minimum speed of impeller N_{js}

$$N_{js} = S \times v^{0.1} \times \left[g \times \frac{(\rho_s - \rho_l)}{\rho_l} \right]^{0.45} \times C_w^{0.13} \times d_p^{0.2} \times D_a^{-0.85} \quad (4.2)$$

In [35] the Zwietering constant S

$$S = 10.42 \left[\frac{C}{D_{in}} \right]^{0.455} \left[\frac{H_L}{D_{in}} \right]^{-0.107} \quad (4.3)$$

C impeller Clearance = 112 mm

Liquid Level $H_L = 552 \text{ mm}$

Vessel Diameter $D_{in} = 496 \text{ mm}$, Substituting all the variables in eq (4.3)

$$S = 5.219$$

Gravity constant $g = 9.81 \text{ m/s}^2$

Kinematic viscosity of water $\nu = 1.004 \times 10^{-6} \text{ m}^2/\text{s}$

Substituting all the variables in eq (4.2),

$$N_{js} = 1.52 \text{ rps (91.347 rpm)}$$

Reynolds number for minimum speed of impeller N_{js} is 1.52 rps,

$$Re = \frac{N_{js} D_a^2 \rho_m}{\mu_m} \quad (4.4)$$

Reynolds number for minimum speed of impeller by substituting the variables $N_{js}, \rho_m, \mu_m, D_a$ in eq (4.4) the Re is 827

From the Figure 19, curve 3 represents the 6 pitched blade impeller, the Power number Po is 1.7 calculated from the intersection point of curve 3 and Re

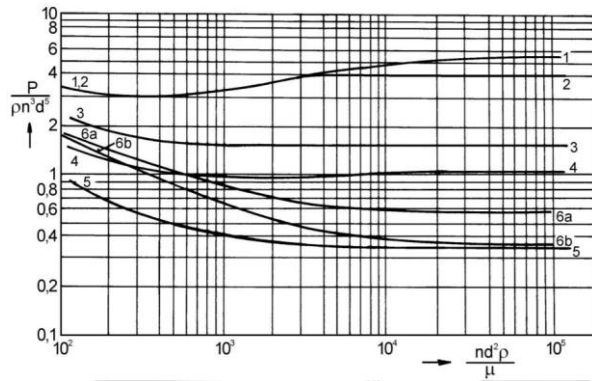


Figure 19 Power number vs Reynolds Number [58]

$$Po = \frac{P}{N_{js}^3 D_a^5 \rho_m} \quad (4.5)$$

Power consumption for minimum speed of impeller P is 0.7908 W

Based on the same calculation procedure for 2 mm particles the minimum speed of impeller N_{js} is 4.22 rps (253.325 rpm) and power consumed P is 22.74 W.

1.4. Shaft diameter calculation

In [36] the rated torque is calculated using the installed electric motor's rated power and the mixers spindle speed. Previously the power consumption for minimum speed of impeller is calculated for both the particle size but calculating shaft diameter it is necessary to select an electric motor and we need to use that motor power during the calculation. So, we choose an electric motor with the power consumption of P_m is 250 W and with a minimum spindle speed of N_{js} is 1.52 rps. Substituting in eq (4.6)

$$M_{km} = \frac{P_m}{2\pi N_{js}} \quad (4.6)$$

$$M_{km} = 26.169 \text{ Nm}$$

In [36] when the torque reaches K times the rated torque of the electric motor, the electrical protection is turned off, according to the category of light operation. The maximum torque on the shaft is then applied.

$$M_k = K_1 M_{km}, \quad K_1 = 1.8 \quad (4.7)$$

$$M_k = 47.105 \text{ Nm}$$

Force acting on blade

$$F = \frac{8 M_k}{3D_a} \quad (4.8)$$

$$F = 759.76 \text{ N}$$

Bending moment

$$M_0 = F * l_1 \quad \therefore l_1 = 0.7 \text{ m unloading length of shaft} \quad (4.9)$$

$$M_0 = 531.836 \text{ Nm}$$

Reduced Torque

$$M_{red} = \sqrt{M_0^2 + \frac{3 M_k}{4}} \quad (4.10)$$

$$M_{red} = 531.869 \text{ Nm}$$

The material used for shaft is EN 1.4301 – Yield strength for temperature 100 °C is 190 MPa and with a safety factor K is 1.5

$$\sigma_{kt} = \frac{R_p 1.0}{K}$$

$$\sigma_{kt} = 126.666 \text{ Mpa}$$

$$d = \sqrt[3]{\frac{32 M_{red}}{\pi \sigma_{kt}}} \quad (4.11)$$

Diameter of shaft, $d = 35 \text{ mm}$

Based on the same calculation procedure for 2 mm particle the diameter of shaft, d is 25 mm.

1.5. Net positive suction head (NPSH)

The available net positive suction is calculated based on the relation between the pressure on the pump suction side to the density of the slurry by gravitational flow, and it is more important to know the available positive suction head to avoid cavitation or phase change.

Let us consider the vapor pressure P_{vp} at this point it depend on the working temperature 80 °C and the vapor pressure (from steam table for 80 °C) P_{vp} is 47.36 kPa. The static head h_s is the height difference between the mixing tank slurry surface and the pump inlet. We can consider the mixing tank of the slurry surface for the maximum height H is 552 mm and the height between the mixing tank bottom and the pump inlet is 433 mm. So, the static head h_s is 985 mm as shown in Figure 18. Towards the suction side, it is necessary to calculate the frictional losses. On the suction side the total length of pipe is 927 mm and frictional loss is calculated from eq (3.3) for pipe. Therefore, the frictional loss in pipe is e_z is 0.406 J/kg. the other two parameters are one diaphragm valve the frictional loss e_z is 0.857 J/kg from eq (3.5) and one elbow the frictional loss e_z is 0.354 J/kg from eq (3.5). The total frictional loss at suction side e_{zs} is 1.617 J/kg. Let assume P_1 as atmospheric pressure at slurry surface of the mixing tank. Velocity of the flow V_D is 0.863 m/s since we are pumping the slurry from the mixing tank to the storage tank.

Substituting the variables $\rho_m, P_1, e_{zs}, P_{vp}, V_D$ in eq (3.13) the pressure at suction side P_s is 62984.34 Pa.

The net positive suction side can be calculated by substituting the variables P_s, ρ_m, g in eq (3.12) the available $NPSH_a$ is 5.99 m.

Based on the same calculation procedure for coarse particles 2 mm the pressure at suction side P_s is 50242.62 Pa and the available $NPSH_a$ is 3.56 m.

Chapter V – Heating units

The slurry is heated with steam at 2 bar pressure to an output temperature of 80 degrees Celsius, and the entire experimental setup should not be longer than 10 meters. The development of heating units is required as a result of this situation.

1. Double pipe heat exchanger

The most basic sort of heat exchanger is a double pipe heat exchanger with two pipes as shown in Figure 20. They are typically used as simple exchangers in numerous sectors. It is great for small projects because it is affordable to design and maintain. They are, on the other hand, less efficient than shell and tube exchangers. They can work in two forms of flow: co-current and counter current. In [41] the counter current approach involves steam and slurry entering in the opposing direction of the flow. Co-current flow occurs when a heating medium runs along the slurry. Because of the largest amount of mass or heat transmission, the counter current is frequently chosen.

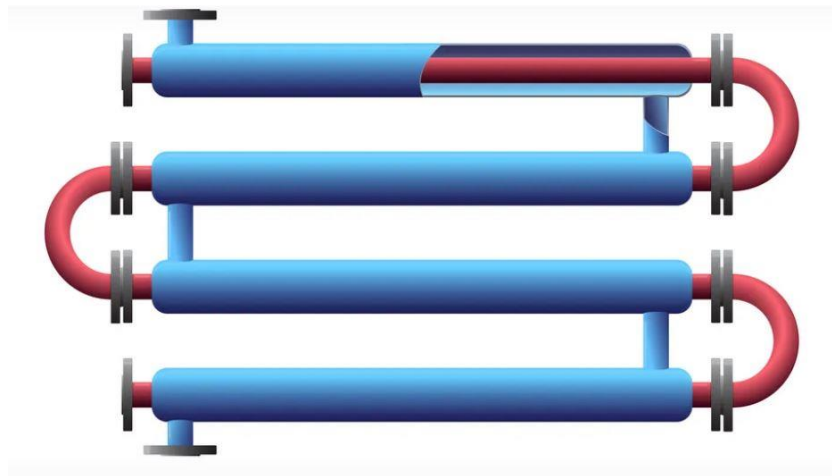


Figure 20 Double pipe heat exchanger [59]

From given condition steam temperature T_s at 2 bar pressure,

$$T_s = 120.23 \text{ }^\circ\text{C}$$

Assuming the atmospheric temperature as the inlet temperature, then the slurry inlet temperature as $T_1 = 20 \text{ }^\circ\text{C}$ and slurry outlet temperature as $T_2 = 80 \text{ }^\circ\text{C}$. Considering pipe as 60.3 x 2 mm (D_1 is 56.3 mm & D_2 is 60.3 mm) with mass flow rate of slurry $m_s = 2.303 \text{ kg/s}$. Thermal

conductivity of stainless steel $\lambda_s = 15 \text{ W/m.K}$, and latent heat of steam $h_e = 2201.6 \text{ kJ/kg}$.
Specific heat capacity of water $C_{pw} = 4.184 \text{ kJ/kg.K}$.

In [40] the properties of steam at 120.23 ° C

Density of steam $\rho_v = 1.27 \text{ kg/m}^3$

Dynamic viscosity of steam $\mu_s = 0.00001296 \text{ Pa.s}$

Thermal conductivity of steam $\lambda_{st} = 0.027496 \text{ W/m.K}$

Enthalpy of liquid phase Δ_{hl} is 504.79 kJ/kg and enthalpy of vapor phase Δ_{hv} is 2706.3 kJ/kg

$$\Delta_{hvl} = \Delta_{hv} - \Delta_{hl}$$

Enthalpy of vapor and liquid phase Δ_{hvl} is 220150 J/kg

Note: Slurry contains both water and glass bead particles for the calculation part assuming only water

Calculation of heat duty Q , related to the mass flow rate of slurry and specific heat capacity of water with temperature difference.

$$Q = m_s C_{pw} \Delta T \quad \therefore \Delta T = T_2 - T_1 \quad (5.1)$$

Substituting the variables $m_s, C_{pw}, \Delta T$ in eq (5.1)

$$Q = 578.21 \text{ kW}$$

Required amount of steam flow rate m_{st} for heating the slurry,

$$m_{st} = \frac{Q}{h_e} \quad (5.2)$$

Substituting the variables Q, h_e in eq (5.2), the mass flow rate of steam m_{st} is 0.2626 kg/s

Total thermal resistance R_{Total} by mean logarithmic temperature difference ΔT_m and heat duty rate Q ,

$$R_{Total} = \frac{\Delta T_m}{Q} \quad (5.3)$$

Mean logarithmic temperature difference,

$$\Delta T_m = \frac{(T_2 - T_1)}{\ln \frac{(T_s - T_1)}{(T_s - T_2)}} \quad (5.4)$$

Substituting the variables T_1, T_2, T_s in eq (5.4)

$$\Delta T_m = 65.73 \text{ }^\circ\text{C}$$

Substituting the variables $\Delta T_m, Q$ in eq (5.3)

$$R_{Total} = 0.0001136 \text{ K/W}$$

The total thermal resistance R_{Total} can be expressed as the sum of the thermal resistance of steel, water, and steam.

$$R_{Total} = R_{steam} + R_{water} + R_{steel} \quad (5.5)$$

Thermal resistance for steam condensing on the surface of the tube wall R_{steam} and the length of tube calculated along the thermal resistance

$$R_{steam} = \frac{1}{\alpha_s A_s} \quad \therefore A_s = \pi D_2 L \quad (5.6)$$

In [39] that the initially estimating heat transfer coefficient of steam $\alpha_s = 8000 \text{ W/m}^2\text{K}$

For calculating the condensing surface area of the tube A_s , the diameter of the tube D_2 is 60.3 mm and the length of the tube L is calculated along the thermal resistance of the steam. By substituting the variables α_s, A_s in eq (5.6)

$$R_{steam} * L = 0.00066 \text{ K.m/W}$$

Thermal resistance of water side or towards slurry R_{water} (inner side of the tube)

$$R_{water} = \frac{1}{\alpha_w A_w} \quad \therefore A_w = \pi D_1 L \quad (5.7)$$

Note: Actually, there will be glass particles in the slurry, so the conductivity will differ with the amount of particles. So, we can assume water for calculation with average temperature 50°C.

Heat transfer coefficient of water α_w is calculated based Nusselt number correlation Nu

Velocity of the flow u ,

$$u = \frac{m_s}{\rho_m A_1} \quad \therefore A_1 = \frac{\pi}{4} D_1^2 \quad (5.8)$$

Substituting the variables m_s, ρ_m, A_1 in eq (5.8)

$$u = 0.86 \text{ m/s}$$

Reynolds number Re is calculated to identify the flow regime,

$$Re = \frac{u D_1}{\nu} \quad (5.9)$$

Kinematic viscosity of water at average temperature 50°C the kinematic ν is $0.553 e^{-06} \text{ m}^2/\text{s}$

Substituting the variables u, D_1, ν in eq (5.9) the Re is 87896 it lies in turbulent flow

Prandtl number Pr is the ratio of momentum transfer and heat transfer,

$$Pr = \frac{\nu}{a} \quad (5.10)$$

Thermal diffusivity of water at average temperature 50 °C the diffusivity a is $0.1551 e^{-06} \text{ m}^2/\text{s}$

Substituting the variables a, ν in eq (5.10) the Pr is 3.57

In [38] the Gnielinski's correlation for turbulent flow through pipes for Nusselt number Nu ,

$$Nu = \frac{Re Pr \xi / 8}{1 + 12.7 \sqrt{\xi} / 8 (Pr^{2/3} - 1)} \left[1 + \left(\frac{d}{L} \right)^{2/3} \right] \quad (5.11)$$

Limits: $10^4 \leq Re \leq 10^6$ and $0.6 \leq Pr \leq 1000$

In [38] the Konakov equation expressed as

$$\begin{aligned} \xi &= (1.8 \log Re - 1.5)^2 \\ \xi &= 0.0182 \end{aligned} \quad (5.12)$$

Substituting the variables Re, Pr, ξ in eq (5.11), the Nusselt number Nu is 395.47

The Nusselt number Nu is the ratio between convective and conductive heat transfer.

$$Nu = \frac{\alpha_w D_1}{\lambda_w} \quad (5.13)$$

Thermal conductivity of water at 50 degree Celsius $\lambda_w = 0.6406 \text{ W/m.K}$

Substituting the variables Nu , λ_w and D_1 in eq (5.13) the heat transfer coefficient of water α_w is 4499.84 W/m²K

For calculating the water flowing surface area of the tube A_w , the diameter of the tube D_1 is 56.3 mm and the length of the tube L is calculated along the thermal resistance of the water. By substituting the variables α_w, A_w in eq (5.7)

$$R_{water} * L = 0.00126 \text{ K.m/W}$$

Thermal resistance of steel side R_{steel} ,

$$R_{steel} = \frac{\ln \frac{(D_2)}{(D_1)}}{2 \pi \lambda_s L} \quad (5.14)$$

Similarly, for the thermal resistance of steel, the total length of the tube is unknown by substituting the known variables D_2, D_1, λ_s in eq (5.14)

$$R_{steel} * L = 0.000728 \text{ K.m/W}$$

Using eq (5.5) it is modified for thermal resistance per length of tube, by substituting the variables R_{steel}, R_{water} and R_{steam} in eq (5.5), we can obtain $R_{total} = \frac{1}{L} (0.0026)$ and we already know the R_{total} which is previously calculated based on heat duty and temperature. By substituting it the total length of the double pipe heat exchanger L is 23.26 m

Overall heat transfer coefficient U ,

$$U = \frac{1}{R_{total} A_2} \quad \therefore A_2 = \pi D_2 L \quad (5.15)$$

Substituting the variables R_{total}, A_2 in eq (5.15), the overall heat transfer coefficient U is 1996 W/m²K

Steam condensing on horizontal tube surface wall,

Wall temperature T_w steam side,

$$Q = \alpha_s A_2 (T_s - T_w) \quad (5.16)$$

$$T_w = 103.83^\circ\text{C}$$

Saturated water at average temperature T ,

$$T = 0.5 * (T_w + T_s) \quad (5.17)$$

$$T = 112.03^\circ\text{C}$$

In [40] the condensate for the saturated water at 112.03°C

Density of water $\rho_l = 949.4 \text{ kg/ m}^3$

Specific heat capacity of water $C_{pw} = 4.23 \text{ kJ/kg K}$

Dynamic viscosity of water $\mu_l = 0.00025 \text{ Pa. s}$

Thermal conductivity of water $\lambda_w = 0.682 \text{ W/m K}$

In [37] using Nusselt model we can calculate the average heat transfer coefficient of steam

$$\alpha_s = 0.725 \left[\frac{(\rho_l - \rho_v) \rho_l g \Delta_{hvl} \lambda_w^3}{\mu_l (T_s - T_w) D_2} \right]^{1/4} \quad (5.18)$$

Substituting the variables $\rho_l, \rho_v, g, \Delta_{hvl}, \lambda_w, \mu_l, T_s, T_w$ in eqn (5.18)

$$\alpha_s (0) = 9114.37 \text{ W/m}^2\text{K}$$

By iteration method replacing heat transfer coefficient of the steam and parallelly the length of the tube calculated according to the procedure described on previous pages.

$$\alpha_s (1) = 9436.76 \text{ W/m}^2\text{K} \quad L (1) = 22.55 \text{ m}$$

$$\alpha_s (2) = 9445.68 \text{ W/m}^2\text{K} \quad L (2) = 22.38 \text{ m}$$

$$\alpha_s (3) = 9429.63 \text{ W/m}^2\text{K} \quad L (3) = 22.37 \text{ m}$$

$$\alpha_s (4) = 9425.13 \text{ W/m}^2\text{K} \quad L (4) = 22.38 \text{ m}$$

$$\alpha_s (5) = 9424.89 \text{ W/m}^2\text{K} \quad L (5) = 22.38 \text{ m}$$

During $\alpha_s (5)$ & $L (5)$ it converges we can stop the iteration at this point.

The double pipe heat exchanger is not acceptable due to its length $L = 22.38 > 10 \text{ m}$. So, the condensing surface area for the obtained length of the tube A_s is 4.24 m^2 .

By substituting the variables $\alpha_s (5), A_s, \Delta T_m$ in eq (5.16) the heat duty rate Q is 2627 kW and the required amount of steam for heating is calculated by substituting the variables Q, h_e in eq (5.2) m_{st} is 1.19 kg/s .

High concentrated suspension of coarse particles 2 mm

Based on the same calculation procedure for 2 mm particles the heat duty rate Q is 2687 kW, the total thermal resistance R_{Total} is 0.0000245 K/W, the Nusselt number by Gnielinski's correlation Nu is 1128, the heat transfer coefficient of water α_w is 12835.77 W/m²K, the length of the tube L is 74.75 m, the overall heat transfer coefficient U is 2887 W/m²K,

After the iteration process, the heat transfer coefficient of steam α_s is 8298.72 W/m²K, the required mass flow rate of steam m_{st} is 3.46 kg/s, the heat duty rate Q is 7623 kW, the length of tube for double pipe heat exchanger L is 73.77 m. Length is greater than the acceptable length, so it is not possible to perform.

2. Shell and tube heat exchanger

In oil refineries and other big chemical processing businesses, shell and tube heat exchangers are the most frequent form of heat exchanger. This form of heat exchanger has a shell with a bundle of tubes inside it, as the name suggests as shown in Figure 21. Patterns of flow, concurrent and countercurrent flow, are two types of twin pipe heat exchangers. Shell and tube exchangers are similar in design to the double pipe or tube in tube exchangers. The fluid to be heated in a shell exchanger is contained in a collection of tube bundles, which are made up of several tubes. In [42] the tube bundles might be fixed tube sheets, U tubes, or a floating head design, and the tubes can be cylindrical or noncylindrical.

In this instance, we are using a single pass setup. A secondary fluid (steam) flows over the tube bundles to heat the fluid inside the tubes (slurry). The tubular heat exchanger is set up in a 1-1 configuration in this instance. In tube bundles, the slurry is the primary fluid, with steam functioning as a secondary fluid to provide heat to the slurry.

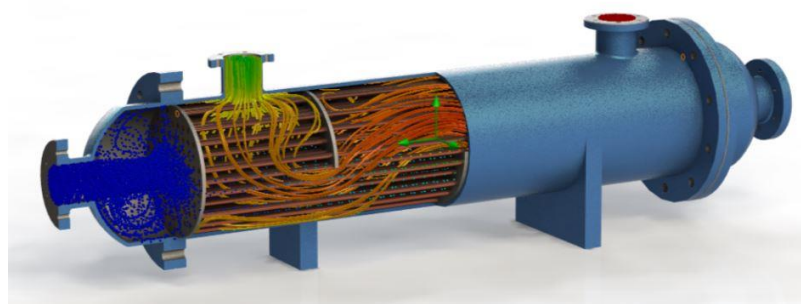


Figure 21 Shell and Tube heat exchanger [60]

Whereas inlet total mass flow rate of slurry m_s is 2.303 kg/s and inlet tube (A) dimension 60.3 x 2 mm. The steel tubing dimension are 18 x 1.5 mm ($D_2 = 18$ mm & $D_1 = 15$ mm). In [39] that the initially estimating heat transfer coefficient of steam α_s is 8000 W/m²K.

Note: The mass flow rate in tube B (18 x 1.5 mm) is calculated similarly as the mass flow rate of tube A (60.3 x 2 mm) by considering the deposition velocity of the flow and the calculation part carried only for single tube B to know whether the length of the tube is less than the expected length of 10 m.

Based on that the mass flow rate of slurry in tube B, $m_b = 0.105$ kg/s. For calculating the no of tubes N_t we can directly divide the mass flow rate in tube A & B because at this flow rate the particles do not settle down in the flow system which is expressed in pumping flow method during pump power calculation.

$$\text{No of tubes, } N_t = \frac{\text{Mass flow rate in tube A}}{\text{Mass flow rate in tube B}}$$

Substituting the variables m_b, m_s in N_t

$$\text{No of tubes } N_t = 22$$

$$\text{Tube pitch } P_T = 1.25 D_2$$

$$P_T = 22.5 \text{ mm}$$

Internal diameter of the shell is based on tube pitch P_T , no of tubes N_t and square arrangement of tubes in tube sheet

$$D_e = 2 P_T \sqrt{\frac{N_t}{\pi}} \quad (5.19)$$

Substituting the variables P_T, N_t in eq (5.19) the internal diameter of shell D_e is 118.79 mm.

Heat transfer coefficient of water α_w

Velocity of inlet slurry flow,

$$u = \frac{m_s}{\rho_m N_t A_1} \quad \therefore A_1 = \frac{\pi}{4} D_1^2 \quad (5.20)$$

$$u = 0.5529 \text{ m/s}$$

Reynolds number Re is calculated to identify the flow regime,

Substituting the variables u, D_1, ν in eq (5.9) the Re is 14996 it lies in turbulent flow

Prandtl number Pr is 3.57 same as from previous pages calculation.

Nusselt number Nu

$$\text{Limits : } 10^4 \leq Re \leq 10^6 \text{ and } 0.6 \leq Pr \leq 1000$$

$$\xi = 0.0276 \quad \therefore \text{Konakov's equation eq (5.12)}$$

$$Nu = 92.52 \quad \therefore \text{Gnielinski's correlation eq (5.11)}$$

Substituting the variable Nu, λ_w and D_1 in eq (5.13) the heat transfer coefficient of water α_w is 3951.44 W/m²K

The total thermal resistance R_{Total} , that the procedure of calculation is the same as in the previous chapter, but with different diameter and thickness of the tube. Using eq (5.5) it is modified for thermal resistance per length of tube we can obtain as,

$$R_{total} = \frac{1}{L} (0.009515)$$

Thermal effectiveness method NTU correlation,

$$NTU = -\ln(1 - \epsilon) \quad (5.21)$$

$$\epsilon = \frac{(T_1 - T_2)}{(T_1 - T_s)}$$

$$\epsilon = 0.5986$$

$$NTU = 0.9128$$

$$NTU = \frac{K S}{W_{weaker}} \quad (5.22)$$

We can calculate heat capacity of Weaker stream i.e., Water

Specific heat capacity of water at average temperature 50 degree Celsius $C_{pw} = 4181 \text{ J/kg K}$

$$W_{weaker} = m_b C_{pw} \quad (5.23)$$

$$W_{weaker} = 439.86 \text{ W/K}$$

$$NTU = \frac{1}{R_{total} W_{weaker}} \quad (5.24)$$

From eq (5.24) the required length of the tube is calculated by substituting the variables $R_{total}, W_{weaker}, NTU$ the length of the tube L is 3.82 m and substituting the length to $R_{total} = \frac{1}{L} (0.009515)$ we can obtain R_{total} as 0.002491 K/W

Steam condensing on horizontal tube surface wall,

From eq (5.1) by substituting the variables $m_b, C_{pw}, \Delta T$ the heat duty rate for a single tube Q is 26.39 kW

Wall temperature T_w of the steam side,

$$Q = \alpha_s A_2 (T_s - T_w)$$

$$T_w = 104.96^\circ\text{C}$$

Saturated water at average temperature T ,

$$T = 0.5 * (T_w + T_s)$$

$$T = 112.59^\circ\text{C}$$

In [40] the condensate (saturated water) at 112.59°C

Density of water $\rho_l = 948.96 \text{ kg/m}^3$

Specific heat capacity of water $C_{pw} = 4.23 \text{ kJ/kg K}$

Dynamic viscosity of water $\mu_l = 0.000248 \text{ Pa.s}$

Thermal conductivity of water $\lambda_w = 0.682 \text{ W/m K}$

In [37] using the Nusselt model we can calculate the average heat transfer coefficient of steam and average number of tube rows in vertical direction $N_a = 4$

$$\alpha_s = 0.725 \left[\frac{(\rho_l - \rho_v) \rho_l g \Delta_{hvl} \lambda_w^3}{\mu_l N_a (T_s - T_w) D_2} \right]^{1/4} \quad (5.25)$$

The properties of steam at 120.23 ° C was already expressed during the double pipe heat exchanger part and it follows the same properties because the steam temperature is the same.

Substituting the variables $\rho_l, \rho_v, g, \Delta_{hvl}, \lambda_w, \mu_l, T_s, T_w, N_a$ in eq (5.25)

$$\alpha_s (0) = 8887.11 \text{ W/m}^2\text{K}$$

By iteration method replacing heat transfer coefficient of steam α_s and parallelly the length of the tube L is calculated according to the procedure described on previous pages.

$$\alpha_s (1) = 9132.381 \text{ W/m}^2\text{K} \quad L (1) = 3.73 \text{ m}$$

$$\alpha_s (2) = 9140.976 \text{ W/m}^2\text{K} \quad L (1) = 3.71 \text{ m}$$

$$\alpha_s (3) = 9129.955 \text{ W/m}^2\text{K} \quad L (2) = 3.71 \text{ m}$$

$$\alpha_s (4) = 9126.752 \text{ W/m}^2\text{K} \quad L (3) = 3.71 \text{ m}$$

By this point we can stop the iteration process step. We can see it convergence both the heat transfer coefficient of steam α_s is $9126.75 \text{ W/m}^2\text{K}$ and the length of tube L is 3.71 m .

Required heat transfer surface area

$$S = \pi D_2 L$$

$$S = 0.21 \text{ m}^2$$

Total heat transfer rate, considering there are 22 tubes

$$Q = \alpha_s S N_t \Delta T_m \quad (5.26)$$

$$Q = 2769.6 \text{ kW}$$

Substituting the variables Q , h_e in eq (5.2), required mass flow rate of steam m_{st} is 1.258 kg/s

Heat exchanger is acceptable due to its length $L = 3.71 < 10 \text{ m}$

High concentrated suspension of coarse particles 2 mm

Based on the same calculation procedure for 2 mm particles the heat duty rate Q is 112.6 kW , the total thermal resistance R_{Total} is 0.00054 K/W , the Nusselt number by Gnielinski's correlation Nu is 429.37 , the heat transfer coefficient of water α_w is $18337 \text{ W/m}^2\text{K}$, the length of the tube L is 9.89 m , the overall heat transfer coefficient U is $3335.2 \text{ W/m}^2\text{K}$,

After the iteration process, the heat transfer coefficient of steam α_s is $7633 \text{ W/m}^2\text{K}$, the required mass flow rate of steam m_{st} is 2.86 kg/s , the heat duty rate Q is 6299 kW , the length of tube for double pipe heat exchanger L is 10.09 m . Even though the length of the tube approximately equal to the required length, on the other hand we need to consider other

constructional parts such as torispherical, nozzles, tube sheet and flanges. Due to this, the length of the overall shell and tube heat exchanger is greater than the acceptable length, so it is not possible to perform.

3. Jacket vessel heating

In terms of efficiency, product quality, and control. The jacket vessel heating technique delivers outstanding heat transfer. The heat transfer medium's velocity and temperature can be precisely regulated. For heating medium, as well as steam and other high-temperature vapor circulation, any type of liquid can be employed. Essentially, we are using steam as a heating medium to condense on a vessel's cylindrical surface. In [43] it is reported that it increases the homogeneity efficiency of fluid properties by adding agitation in jacketed vessels, allowing for further uniform temperature or concentration levels.

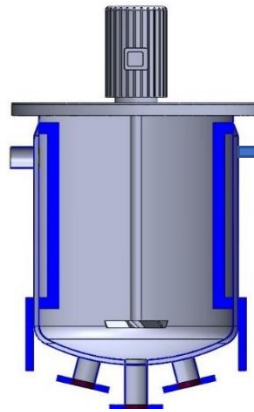


Figure 22 Jacketed vessel

Jacketed vessel types

In [44] the types of jacketed vessels are mentioned below.

Conventional jacket: an external shell is added over the vessel, creating an annular area through which the heating medium flows as shown in Figure 22. Suitable for high volume fluids and optimum for small capacity vessels.

Half coil pipe: it is welded around the vessel to allow the heating medium to circulate along the exterior of the tank, it is perfect for determining the wall thickness for construction that saves money on materials. It is best for high-temperature industrial procedures, and the price is in the center.

Dimple jacket: Spot welds form a thin shell around the vessel in the case of dimple vessel jackets. Dimple jackets enable light-gauge metal construction without sacrificing the strength and durability needed to withstand internal vessel pressure. Larger vessels should have a cheaper pricing.

In chapter 2 during mixing tank calculation, we considered the volume of tank V is 0.1 m^3 , the density of the slurry ρ_m is 1071.45 kg/m^3 , the height of the tank H is 552 mm and the diameter of tank D_{in} is 496 mm . In chapter 4 it is calculated that the diameter of the impeller D_a is 0.165 m and the minimum speed of impeller N_{js} is 1.52 rps

Total amount of slurry to be heated up by steam,

$$\begin{aligned} \text{Mass of slurry } m &= \rho_m V \\ m &= 107.145 \text{ kg} \end{aligned}$$

Steam (saturated) condensing on the cylindrical surface of a vessel is used to heat a mass of slurry m is 107.145 kg from an initial temperature of T_1 is 20°C to a final temperature of T_2 is 80°C . In a cylindrical vessel with a dished end bottom, the product is heated. Pitch blade impellers are ideal for agitating slurry. Baffles are installed on the cylindrical surface of a vessel to improve mixing.

Heat transfer surface area,

$$S = \pi D_{in} H = 0.8600 \text{ m}^2$$

Now we must calculate the heat transfer coefficient on the agitated side as well as the condensing steam side. The temperature of the agitated liquid changes during heating, i.e., the properties of the liquid change and both heat transfer coefficients change. We can divide the temperature intervals for heating (i.e., $20^\circ\text{C} \rightarrow 80^\circ\text{C}$) into lot of smaller intervals, i.e., $20 - 25^\circ\text{C}$, $25 - 30^\circ\text{C}$,, $75 - 80^\circ\text{C}$, For first case ($20 - 25^\circ\text{C}$). Typically, the engineering approach is to use properties at average temperature 22.5°C .

Reynolds number for impeller Re ,

$$Re = \frac{N_{js} D_a^2}{\nu} \tag{5.27}$$

Kinematic viscosity of water at the average temperature of 22.5 °C and the kinematic viscosity ν is $0.923 e^{-06} \text{ m}^2/\text{s}$. The thermal diffusivity of water at average temperature 22.5 °C a is $0.150 e^{-06} \text{ m}^2/\text{s}$.

$$Re = 45032.147$$

From eq (5.10) by substituting the variables a, ν the Pr is 6.16

Nusselt number correlation for pitch blade impeller,

In [38] for a baffled vessel

$$Nu = 0.66 (\sin \gamma)^{0.5} Re^{2/3} Pr^{1/3} \quad (5.28)$$

$$\gamma = 45^\circ$$

$$\text{Limits : } 10^2 \leq Re \leq 4 \times 10^5 \text{ and } 2 \leq Pr \leq 2 \times 10^3$$

$$Nu = 1412.758$$

$$Nu = \frac{\alpha_w D_{in}}{\lambda_w}$$

Thermal conductivity of water at 22.5 °C λ_w is 0.60857 W/m K

$$\alpha_w = 1733.391 \text{ W/m}^2\text{K}$$

At this point, I must state that continuing to calculate the heat transfer coefficient on the steam condensing side is not necessary from an engineering standpoint. Why? During condensation, the heat transfer coefficient is on the order of 10000 W/m²K. In comparison to convective thermal resistance on the agitated liquid side, thermal resistance on this side can be ignored.

But we will continue with Condensing steam side α_s ,

In [39] the Estimation of heat transfer coefficient of steam α_s is 10000 W/m²K

Liquid height $H = 0.552 \text{ m}$ and thickness of tank $T = 2 \text{ mm}$

Inner surface area $S_{in} = \pi D_{in} H, \quad \therefore D_{in} = 496 \text{ mm}$

$$S_{in} = 0.860 \text{ m}^2$$

Outer surface area $S_o = \pi D_o H, \quad \therefore D_o = 500 \text{ mm}$

$$S_o = 0.866 \text{ m}^2$$

Thermal conductivity of stainless steel, $\lambda_s = 15 \text{ W/m K}$

Overall thermal resistance of heat transfer surface,

$$R_{total} = \frac{1}{K S} = \frac{1}{\alpha_w S_{in}} + \frac{\ln \frac{(D_o)}{(D_{in})}}{2 \pi \lambda_s H} + \frac{1}{\alpha_s S_o} \quad (5.29)$$

$$R_{total} = 0.000941 \text{ K/W}$$

Heat duty rate Q

Note: Temperature difference will differ with actual temperature in vessel, on the other hand calculation is non-stationary process,

$$T_{avg} = \frac{T_1 + T_2}{2} = 22.5^\circ\text{C}$$

$$Q = \frac{\Delta T}{R_{total}} \quad \Delta T = T_s - T_{avg}$$

$$Q = 103.904 \text{ kW}$$

Wall temperature T_w steam side and the temperature of steam T_s is 120.23°C . Substituting the variables α_s, S_o, Q, T_s in eq (5.16) the wall temperature of steam side T_w is 108.24°C

Saturated water at average temperature T , by substituting the variables T_w, T_s in eq (5.17) the average temperature of saturated water T is 114.237°C

Condensing steam side,

In [38] mentioned that for the Nusselt model (α_s) of laminar condensation

$$\alpha_s = 0.943 \left[\frac{(\rho_l - \rho_v) \rho_l g \Delta_{hvl} \lambda_w^3}{4 \mu_l (T_s - T_w) H} \right]^{1/4} \quad (5.30)$$

The properties of steam at 120.23°C was already expressed during the double pipe heat exchanger part and it follows the same properties because the steam temperature is the same.

In [40] the condensate (saturated water) at 114.237°C

Density of water $\rho_l = 947.7 \text{ kg/m}^3$

Specific heat capacity of water $C_{pw} = 4.23 \text{ kJ/kg K}$

Dynamic viscosity of water $\mu_l = 0.00024 \text{ Pa. s}$

Thermal conductivity of water $\lambda_w = 0.682 \text{ W/m K}$

Substituting the variables $\rho_l, \rho_v, g, \Delta_{hvl}, \lambda_w, \mu_l, T_s, T_w$ in eqn (5.30)

$$\alpha_s(1) = 5237.11 \text{ W/m}^2\text{K}$$

By Iteration process and we can repeat with calculation $R_{total}, Q, \alpha_s, \dots\dots$

$$\alpha_s(2) = 4531.91 \text{ W/m}^2\text{K}$$

$$\alpha_s(3) = 4394.14 \text{ W/m}^2\text{K}$$

$$\alpha_s(4) = 4365.66 \text{ W/m}^2\text{K}$$

$$\alpha_s(5) = 4359.65 \text{ W/m}^2\text{K}$$

$$\alpha_s(6) = 4359.51 \text{ W/m}^2\text{K}$$

Convergence takes place at $\alpha_s(6)$ iteration. So, we can stop future iteration steps.

Overall thermal resistance of heat transfer surface, we can substitute heat transfer coefficient value obtained during the iteration process considering the converged heat transfer coefficient α_s is $4359.51 \text{ W/m}^2\text{K}$. Based on that by substituting the variables $\alpha_w, S_{in}, \lambda_s, H, \alpha_s, S_o, D_o, D_{in}$ in eq (5.29) the overall thermal resistance R_{total} is 0.00109 K/W

Heat duty rate Q is calculated after the iteration process by substituting the variable $R_{total}, \Delta T$ in eq (5.3) the heat duty rate Q is 89.676 kW

Finally, we can calculate the time required for the heating,

$$t_{20-25^\circ\text{C}} = \frac{-m C_{pw}}{K S \frac{\ln(T_s - T_2)}{(T_s - T_1)}} \quad (5.31)$$

Substituting the variables $m, C_{pw}, T_s, T_1, T_2, R_{total}$ in eq (5.31) the time $t_{20-25^\circ\text{C}}$ is 25.25 s

Amount of steam required for heating can be calculated by substituting the variables Q, h_e in eq (5.2) the $m_{st\ 20-25^\circ\text{C}}$ is 0.04073 kg/s

Similar procedure is followed for other intervals based on that we can calculate the total time for heating and the total amount of steam required for heating

Total time required for heating from 20 – 80°C

$$t_{20-25^{\circ}\text{C}} + \dots + t_{75-80^{\circ}\text{C}} = 2098.9 \text{ s}$$

Total amount of steam required for heating 20 – 80°C

$$m_{st\ 20-25^{\circ}\text{C}} + \dots + m_{st\ 75-80^{\circ}\text{C}} = 0.3965 \text{ kg/s}$$

High concentrated suspension of coarse particles 2 mm

Based on the same calculation procedure the mass of slurry m is 143.87 kg, the heat duty rate Q is 160.4 kW, the total thermal resistance R_{Total} is 0.00061 K/W, the Nusselt number Nu is 2791, the heat transfer coefficient of water α_w is 3424.58 W/m²K and the heat transfer coefficient of steam α_s is 4665.52 W/m²K.

After the iteration process, the heat transfer coefficient of steam α_s is 3839.78 W/m²K, the heat duty rate Q is 123.04 kW, the total thermal resistance R_{Total} is 0.00079 K/W, the time $t_{20-25^{\circ}\text{C}}$ is 24.66 s, the total time for heating $t_{20-25^{\circ}\text{C}} + \dots + t_{75-80^{\circ}\text{C}}$ is 2105.20 s, the amount of steam required for heating $m_{st\ 20-25^{\circ}\text{C}}$ is 0.0055 kg/s and the total amount of steam required for heating $m_{st\ 20-25^{\circ}\text{C}} + \dots + m_{st\ 75-80^{\circ}\text{C}}$ is 0.0533 kg/s

Still, it is possible to make accurate solution. We can divide the temperature intervals for heating (i.e., 20 → 21 °C) into lot of smaller intervals.

Chapter VI – Experimental stand for flow suspension in pipe flow

1. Experimental setup of slurry flow loop layout

In order to achieve the desired results, an effective and comprehensive methodology must be established, along with a flow loop system that provides for easy measurement, visualization, and validation of slurry flow parameters. The velocity, concentration, and temperature profiles are the most essential characteristics in this investigation.

2. Horizontal slurry flow loop layout

The experimental setup is carried out in an open circuit loop layout with recirculating as shown in Figure 23. The main components are the mixing tank with jacketed vessel, motor, centrifugal pump, diaphragm valves, pressure sensor, electromagnetic flow meter, ERT sensor, thermocouple, and storage tank. The entire length of the horizontal pipelines is 14 m and the vertical pipelines are 2 m with DN 50 pipe. The connecting pipes are made of EN 1.4301 stainless steel. The mixing tank has a 100-liter capacity and is connected to a motor with a pitch blade impeller to produce a homogeneous mixture before being introduced into the loop. As a result, the mixing tank's primary role is to mix and contain the slurry that has returned from the flow loop before pumping it back into the flow loop. The slurry is pumped through the loop by a centrifugal pump and the mean slurry flow rate is maintained by a variable driving frequency, which is connected with the motor to control the speed and the motor is coupled with the centrifugal pump. The electromagnetic flow meter is installed at the start of the flow loop and is 1 meter away from the centrifugal pump's discharge end and helps in the measurement of the flow rate. A pressure transmitter is installed at two different locations. One is installed between the electromagnetic flow meter and the test section, while the other is installed between the test section and the thermocouple. As a result, a pressure transmitter is utilized to prevent pressure loss before the intake or exit of the test section. To measure the temperature of the slurry, a K – type thermocouple is attached to the pipeline. Finally, the slurry is transported to a storage tank and then the flow continues once again.

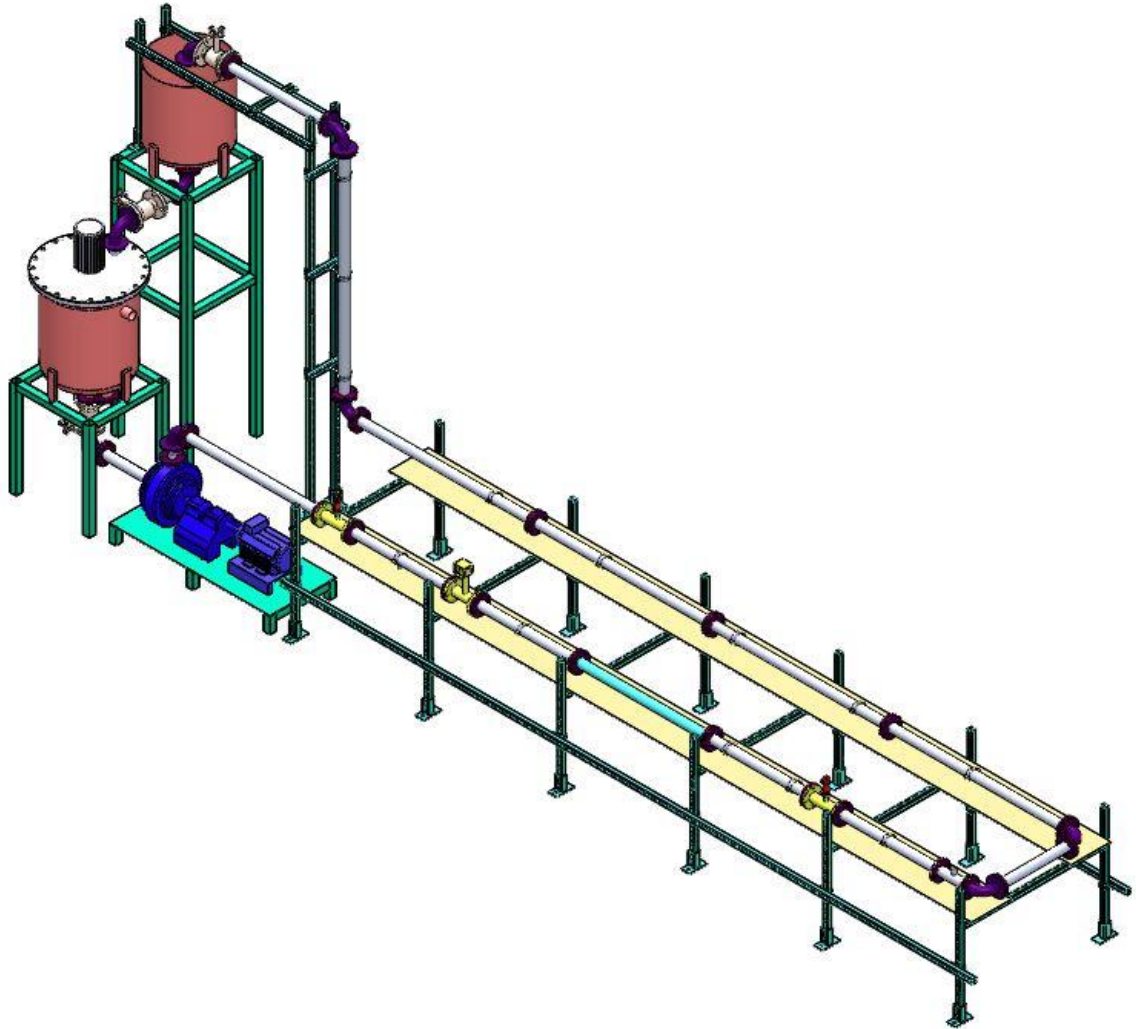


Figure 23 Overall Experimental setup [47]

3. List of devices present inside experimental setup of slurry flow loop layout

3.1. Mixing tank

The mixing tank is coupled with the outer shell known as the jacketed vessel which is used for the heating purpose. The steam is passed through the inlet nozzle of the jacketed vessel and the steam starts to condense on the outer surface layer of the mixing tank. The condensation can take place in two different forms film-wise condensation and drop-wise condensation, but in our model the film-wise condensation method is followed. A film layer is created at the outer layer of the wall of the mixing tank through which heat transfer occurs by the conduction process. During condensation a thin film boundary layer is created, which acts as resistance for heat transfer, but in the calculation part the film boundary layer thickness is neglected. Condensed

vapors are released outside the jacket vessel through an outlet nozzle and steam that is condensed into liquid is also drain out as shown in Figure 24. For the homogenous preparation of mixture, the shaft is coupled with motor by a coupling device and to avoid the friction during the motor and the shaft rotation, a radial bearing housing can be used. The motor is mounted on the top cover, which is mounted to the flat flange by bolts. To avoid reaction forces during mounting between the flat cover and the flat flange, the gasket is used. The baffles help to ensure homogeneous suspension of the particles in the mixing tank. Finally, when the slurry obtains the required temperature, the diaphragm valve is opened for the slurry to flow inside the experimental setup. In the Appendices, the detailed description of the mixing tank construction parts is shown in Ex -10001-JVA and the drawing is shown in Ex -10001- 1- JVD. In Table 7 the detail information is given for flanges, elbow, nuts & bolts.

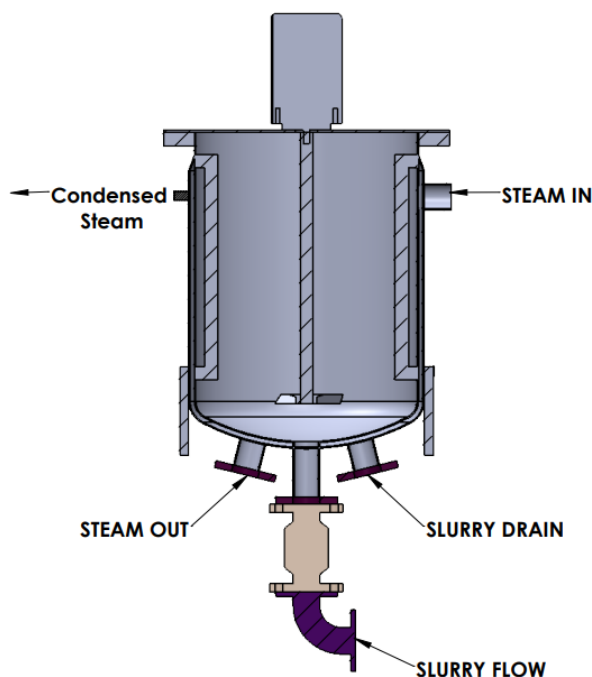


Figure 24 Mixing tank with jacketed

3.2 Supporting system

The supporting system used in this experimental set up is mainly focused on easy to assemble and dismantle in working environment. For this case, the Halfen support stands helped to connect each part with nuts and bolts. Using Halfen stands, the complete pipeline assembly is supported with dismountable supporting system and other storage tank and mixing stand are supported with square tubes which are welded as shown in Appendices Ex- 10000 - MA. A

simple Halfen stand for the pipeline is shown in Figure 25. In the Appendices, the detailed description supporting system for the mixing tank, storage tank, and pipeline assembly is shown in Ex -10004-VHD and the drawing is shown in Exp -10004- 1- STD. In Table 7 the detailed information is given for pipe clamps, clamp rods, nuts & bolts etc.

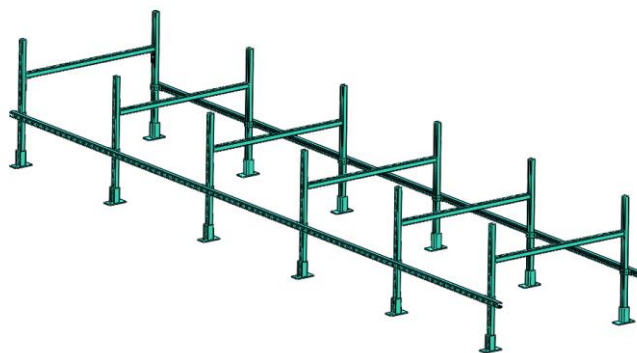


Figure 25 Halfen stand for pipeline system

3.3. Centrifugal pump

Centrifugal pumps are the most prevalent form of slurry pump. Centrifugal pumps use an impeller to move the slurry, and the liquid follows the rotation of the impeller axis. The centrifugal pump, which can handle solids, is utilized in these overall experimental settings. The flow rate and total head are varying based on two different particles. When choosing a pump, it is better to select for the particle that has a higher flow rate and a total head. Because a variable frequency drive that is electrically coupled to the motor may control the pumping flow rate. As a result, the flow rate for 10 microns and 2 mm glass bead particles is 7.738 m³/hr and 26.77 m³/hr respectively. The pump should be chosen based on this circumstance. Based on our flow rate and total head, we choose the Warman 1.5/1 BAH model for both the particles as shown in Figure 26.



Figure 26 Warman slurry pump [61]

3.4. Motor for mixing and pumping

In an overall experimental setup two motors are used as shown in Figure 27. The first motor is used for the homogeneous mixing of the slurry mixture. The second motor is used to drive the centrifugal pump to circulate the slurry mixture throughout the flow loop setup. In our case, we have two different types of particles, as mentioned previously. Therefore, for 10-micron glass beads the minimum power consumption for mixing P is 0.794 W and the power to pump the slurry mixture P is 0.061 kW, but the required electric power input for the motor to pump P_e is 0.086 kW. Similarly, for 2 mm glass beads the minimum power consumption for mixing P is 22.74 W and the power to pump the slurry mixture P is 1.45 kW, but the required electric power input for the motor to pump P_e is 2.1 kW. The detail information about the motor is mentioned in the Table 2.

Table 2 Motor Specification [62]

Position	Particle size	Motor type	Product code	Output kW	Company
Mixing tank	10 μ m, 2 mm	M3BP 71MD4	3GBP072340- BSK	0.25	ABB
Centrifugal pump	10 μ m, 2 mm	M3BP 100LKA 4	3GBP102810- ASK	2.2	ABB



Figure 27 ABB- Flange mounted & Foot mounted motor [62]

3.5. Variable frequency drive

It is an electronic device which controls the speed of the AC induction motor and is a type of motor controller that drives an electric motor by varying the frequency and voltage of its power supply. For our condition, we need to select a variable frequency drive, but ABB recommended the variable frequency drive for the selected motors. In [62] the variable frequency drive used in this experimental setup should be ACQ580-01 as shown in Figure 28.



Figure 28 ABB - Variable frequency drive [62]

3.6. Pressure transmitter

The pressure transmitter is an important parameter because when there is pressure loss in the flow, then there will be settling of particles and blockage of the pipe or damage to the bottom part of the pipe by wear resistance. To avoid this kind of cause, the pressure transmitter is used

to monitor the pressure losses. The pressure transmitter is directly connected to the DAS system. In the experimental setup, the Danfoss pressure transmitter is used as a pressure sensor, as shown in Figure 29. The detail information about the pressure transmitter is mentioned in the Table 3.



Figure 29 Danfoss pressure transmitter [63]

Table 3 Pressure Transmitter specification [63]

Pressure Transmitter Type	Pressure transmitter flush diaphragm MBS 4010
Nom. output signal (short-circuit protected)	4 – 20 mA
Sensor temperature range	- 10 – 85 °C
Measuring Range	0 – 4 bar
Ordering data	MBS 4010-1611-A1CB12-2

3.7. Electromagnetic flow rate meter

Electromagnetic flow meters detect flow by using Faraday's law of induction. Generally, an electromagnetic flow meter is unaffected by the temperature, pressure, viscosity, or density of the liquid. Moreover, it helps to detect the multiphase flow as well as that there is no pressure loss and moving parts. In the overall experimental set-up, only one flow meter is used to monitor the flow rate. In [64] the Siemens flow sensor SITRANS FM MAG 3100 HT can be used as electromagnetic flow rate meter Figure 30 and for transmitters verificatory SITRANS F M Verificator Transmitters MAG 5000/6000 can be used in the experimental setup as shown in Figure 31. The detail information about the electromagnetic flow meter and transmitter is mentioned in the Table 4 & 5.



Figure 30 Siemens electromagnetic flowrate meter [64]

Table 4 Electromagnetic Flowrate Meter Specification [64]

Electromagnetic flowrate meter type	SITRANS FM MAG 3100 HT
Material and Temperature	PTFE: –20 to 150°C
Pressure rating	PN 40
Flange material and standard	Stainless steel, EN 1092-1
Selection and Ordering data	2YF32-1A1



Figure 31 Siemen's transmitter [64]

Table 5 Transmitter Specification [64]

Transmitter Type	SITRANS F M Transmitters MAG 5000/6000
Digital Input	11 ... 30 V DC, Ri = 4.4 KΩ
<ul style="list-style-type: none"> • Activation time • Current 	50 ms 11 V DC = 2.5 mA, 130 V DC = 7 mA
Output	
<ul style="list-style-type: none"> • Signal range • Frequency 	0... 20 mA or 4 ... 20 mA 0 ... 10 kHz, 50 % duty cycle
Selection and Ordering data	7ME6910- 1AA30-1AD0

3.8. Diaphragm valve

The diaphragm valve is best suited for suspension flow characteristics due to the ability to handle solid particles, no dead areas where particles may collect, low resistance coefficient, easy maintenance, and automation. In our case, we can use straight-through-type diaphragm valves. The flow resistance in the straight-through type valve body is lower and the flow performance is better than that in the weir type valve body. In [65] the straight-through type diaphragm valves - DIAVAL® series ST from COMEVAL Valve System is suggested to be used for the experimental setup as shown in Figure 32. The detail information about the diaphragm valve is mentioned in the Table 6



Figure 32 Straight diaphragm valve [65]

Table 6 Diaphragm valve Specification [65]

Diaphragm valve type	Straight Through Type Diaphragm Valves - DIAVAL® Series ST
Flowrate	110 m ³ /h
Temperature range and Material	–10 to 85°C Hard Rubber
Diaphragm Temperature Range	D50 Neoprene Rubber –20 to 95°C

3.9. Temperature measurement

K - type thermocouple is used to monitor the slurry temperature. When there is a change in the temperature of the slurry, the viscosity of the slurry is affected, and this results in a dramatic effect in the flow behavior of the slurry. In this experimental setup, the K-type thermocouple is mounted on a horizontal section of the pipe as shown in Figure 33 and placed next to the second pressure transmitter sensor, where the slurry data is collected. The K-type thermocouple is very commonly used. They are inexpensive and can be used to monitor the temperature range from 0 to 100 ° C. However, we have a device to measure the temperature profile, in addition a thermocouple is used to monitor. In [66] the K-type thermocouple is selected from JARKAR and cartridge diameter size 0.51mm and length 7.5 m with wire insulation of Teflon and product code TT-K-24-SLE-25.



Figure 33 K - type thermocouple [66]

4. List of constructional components for flow loop

Table 7 Constructional Component for flow loop

Item		Dimension	Supplier	Product code	Quantity
DN 50 EN 1.4301 pipe		OD 60.3 X 2 mm	SANDVIK	Sandvik 3R60	14 m
DN 50 Clear Upvc Transparent pipe		OD 60.3 X 2 mm	https://www.bazenysshop.cz/	V0301605128	1.5 m
EN 1092 – 1 Flanges Type 5		DN 500	WELLGROW INDUSTRIES CORP	EN 1092 – 1 PN 10	1
EN 1092 – 1 Flanges Type 1		DN 50	WELLGROW INDUSTRIES CORP	EN 1092 – 1 PN 10	30
PVC Flange		DN 50	GF Piping System	DN 50 PN 10	2
EPDM GASKET		DN 50	https://www.indcom.cz/en/clamp-gasket-ethylen-propylen	GEPDM_50	15
Nuts & bolts		M16 x 80	https://www.cajkservis.cz/	13010	60 Set
Elbow 90		DN 50	https://www.topenilevne.cz/	0008485	6
Pipe clamp & Rod		DN 50	https://www.heiz24.de/	WS9404789	15 set
Constructional stand		-	HALFEN System	HL 36/36	41 m
Constructional stand support		-	HALFEN System	HVT 36 – 7	16
Constructional stand support		-	HALFEN System	HVT 36 – 4	24
Constructional stand support		-	HALFEN System	HVT 36 – 2	12

Result and discussion

The overall experimental setup is based on a literature study, several measurement devices, apparatuses, and equipment. All the measurement device, apparatuses and equipment mention in this thesis results in its own range. Therefore, it is necessary to select the best suitable device, apparatus, and equipment based on their results, which is followed by a discussion of the results.

Non-invasive measurement device

When comparing all techniques, each method is a different and unique way of measuring. Among these, I prefer to choose the electrical resistance tomography technique, because the cost is lower than other techniques and because of the safety precautions. While other techniques such as MRI are expensive and its drawback is that it cannot measure every object, gamma ray and PEPT contain radiation and a high safety measure is required. The X-ray setup is large and cannot be performed as a field measurement. For temperature profile measurement, infrared thermography may be preferable. It gives a better response than TLC and LIF, but still not as good as MRT. The Non-invasive measurements devices are placed in the pipeline system in between the electromagnetic flow meter and the pressure transmitter.

Gravitational and pumping method

The gravitational and pumping methods are almost the same. There are certain differences between them about the placement of the centrifugal pump and the placement of the mixing tank from the bottom. We can see that during the gravitational method, a pump is used to recirculate the slurry to the storage tank from there to the mixing tank. During gravitational flow, the most important thing is to maintain the deposition velocity because we have two different types of particle size and volume concentration and similarly, they have different deposition velocities also. To obtain this velocity through this method, it can be achieved by changing the height of the free flow of the slurry. There is a change in flow rate or any other pressure loss during the flow, and it is complicated to achieve. Because we need to change the height of the free flow and it is complicated to have such an experimental setup with vertical movement of the mixing tank to achieve it. During calculation, the heights of the two different particles vary from each other. Compared with the pumping method, it overcomes all the drawbacks from the gravitational method. Important things are that there is no variation in height of the mixing tank

from bottom to achieve velocity. Because pumps help to achieve the velocity, and when there is a change in flowrate or pressure loss in flow, it can be solved by adjusting pump power.

Double pipe and shell & tube heat exchanger

Although the double pipe heat exchanger is a straightforward technique of heat transfer, it is not suitable for our experimental setup. The major problem with the double pipe heat exchanger in this experimental setup is the overall length of the heat exchanger. The experimental setup should be compact in size with an overall length of 10 meters in maximum. However, we can see through the calculation for different particle sizes that the overall length is greater than the required length. Similarly, for the shell and tube exchanger, the overall length for heat transfer is acceptable for 10-micron particles and for 2 mm particles still the overall length for heat transfer is approximately equal to the required length but during overall construction the length of the overall shell & tube heat exchanger get higher than the required length and there are some possibilities for the settling of glass bead particles due to the pressure drop when the slurry flow strikes on tube sheet and it is not possible to assume the concentration of glass bead particles in each tubes of the bundle. From my point of view, there are some possibilities to reduce the overall length of heat transfer without affecting the deposition velocity. It is possible by reducing the diameter of the slurry flow tubes. However, there is also a problem when we are trying to reduce the size of the tube, it is complicated during the flow of 2 mm particles which cause blockage of tubes.

Jacketed vessel heat exchanger

The jacketed vessel can also be considered as a compact device for heat exchanger. In this experimental setup, a jacketed vessel is used as heating device. Compared to the two other types of heat exchangers, there is no variation in dimensions for the two different types of particles. During the calculation, we can see that there is a change in the total mass of the slurry mixture due to the diameter and volume concentration of the glass bead particles. Due to this, there is a change in time required for overall heating. The heat transfer coefficient for the steam side and the slurry side is lower than those for the other two heat exchangers. The time required for heating the slurry mixture takes approximately around 35 minutes for both particles. Although the initial time required for heating is higher, it is still acceptable because it satisfies the required conditions.

Conclusion and Recommendation

The main aim of this thesis was to design a workable condition of an experimental stand for observation of suspension in flow. Through literature study, we conclude several possible measurement methods or techniques to measure velocity, concentration, and temperature profile. Among that electrical resistance tomography technique for measuring velocity and concentration profiles it has more advantages compared to other techniques such as no radiation emission, the measuring device is not a bigger, it is possible for both field and laboratory measurements, no skilled operators or safety precautions required, it is cost effective, compact size and it gives acceptable results. Although electrical resistance tomography is more advantageous, the results are still not accurate due to its image resolution. For the present experimental setup, it is the best suitable device for measuring velocity and concentration profiles. For the case of temperature profile measurement infrared thermography is suitable.

Through the calculation part it can be concluded that the best fit parameters to the experimental stand. Thanks to the Excel sheets for performing a huge calculation and providing an accurate result. The calculation part helps to avoid the trial and error method for the experimental stand. In the thesis there are several approaches which have been made for the setup of experimental stand as discussed previously about the gravitational and pumping method. In our thesis, we are using the pumping method based on that the experimental stand is designed for the working condition. Therefore, we can optimize the power required for a motor for mixing and to run a pump. On the other hand, for the heating device in this thesis there are three different types of heating elements. All three devices enable heat transfer, but they cannot be chosen randomly or assumed. In this case, the mathematical calculation provides an accurate result of every device. Based on the calculation report, each part was designed for the setup of experimental stand.

A compact experimental stand with all functional unit is made perfectly by CAD modelling software SOLIDWORKS 2016. CAD software helps to view the components in 3D which makes more realistic and get better ideas for fine tune the experimental stand. After designing of each part and they are assembled as shown in Figure 23. The bill of material provides detail information about all components. Finally, the components are dimensioned in drawing sheet and bill of materials is made for future setup of experimental stand as shown in appendices main assembly EX – 10000 – MA, main assembly dimension EX – 10000 –01 – MSD , Jacket vessel assembly EX – 10001 – JVA, Jacket vessel dimension EX – 10001 – 1 – JVD, Pipe line

assembly EX – 10002 – PLA, Pipe line dimension EX – 10002 – 01 – PD, Storage vessel assembly EX – 10003 – SVA, Storage vessel dimension EX – 10003 – 1 – SVD, Stands EX – 10004 – 1 – STD and Vertical and horizontal stand EX – 10004 – 1 – VHD.

Recommendations

It is clear from the literature review that magnetic resonance tomography enables a better result compared to other measurement techniques but unfortunately it requires several conditions for measurement. Once we satisfy all the conditions for MRI, then we can use it for the experimental stand. For the case of jacketed vessel for heating, instead film wise condensation the drop wise condensation can be used for better heat transfer. If dropwise condensation is preferred, the outer surface of the mixing tank should be coated with a silicon or Teflon layer, so the vapor condenses like a droplet and falls due to gravitational force. The calculation for the temperature still it is possible to get more accurate results through stepwise calculation by a different of 1° C or even less to get still accurate results. In this thesis, the different temperature is 5° C, so the approximate results are obtained. For each step wise it contains 6 iterations. So, when it comes to stepwise 1° C, it contains a total of 348 iterations and for both particle cases it will be 696 iterations.

References

- [1] Anil R. Oroskar, Raffi M. Turian - The critical velocity in pipeline flow of slurries – AICHE JOURNAL – July 1980 – Volume 26, Issue 4 – pp 550 – 558, <https://doi.org/10.1002/aic.690260405>
- [2] Randall Gordon Gillies - Pipeline Flow of Coarse Particle Slurries – University of Saskatchewan – October 1993 – pp 7 – 8, <http://hdl.handle.net/10388/etd-03242009-142017>
- [3] Baha E. Abulnaga, P.E. – Slurry Systems Handbook –New York: Mc Graw Hill – 2002.
- [4] J Polansky - Experimental investigation of slurry flow – University of leeds – September 2014 – pp 3 – 6.
- [5] C T Crowe. Fluid-Solid Transport in Ducts: Slurry Flows. Multiphase Flow Handbook – Boca Raton FL: CRC: Taylor & Francis, 2006.
- [6] C A Shook and M C Roco – Slurry Flow: Principles and Practice – Howard Bernner – October 1997, 1st edition.
- [7] Peker, S. M., Helvacı, S., S. Yener, H. B., İközler, B., Alparslan, A. (2008). Solid-Liquid Two Phase Flow – ScienceDirect – 2008.
- [8] A. Averbakh, A. Shauly - Slow viscous flow of highly concentrated suspensions – Part 1: Laser doppler velocimetry in rectangular ducts – Internal journal of Multiphase flow – 1997 Vol 23, Iss 3 – pp 411 – 412.
- [9] K D Jensen -Flow measurements – ENCIT2004 – 10th Brazilian Congress of Thermal Sciences and Engineering, Nov. 29 – Dec. 03, 2004, Vol 26, pp 400 – 401, Rio de Janeiro, RJ, Brazil .
- [10] Christophe Boyer, Anne-Marie Duquenne, Gabriel – Measuring techniques in gas – liquid and gas - liquid – solid reactors – Elsevier – March 2002, pp 3194 – 3915.
- [11] D.J. Parker, C.J. Broadbent, P. Fowles, M.R. Hawkesworth, P. McNeil - Positron emission particle tracking – a technique for studying flow within engineering equipment – Elsevier – 10 March 1993, Vol 326, Issue 3, pp – 592 – 607.

- [12] Olga Mihailova, Victor Lim, Michael J. McCarthy – Lamina mixing in a SMX static mixer evaluated by positron emission particle tracking (PEPT) and magnetic resonance imaging (MRI) – Elsevier – 1 December 2015, Vol 137, pp 1014 – 1023.
<https://doi.org/10.1016/j.ces.2015.07.015>
- [13] Mohamed Ammar Garman - Local Particle Velocity Measurements In Slurry Flow In Pipes And Centrifugal Pumps Using Ultrasound Technique – Case Western Reserve University – January 2015, pp 40 – 42.
- [14] Matthias Messer - Pulsed Ultrasonic Doppler Velocimetry for Measurement Of Velocity Profiles In Small Channels And Capillaries – Georgia Institute of Technology – December 2005
- [15] Kalaga, D.V., Kulkarni, A.V., Acharya, R., Kumar, U., Singh, G., Joshi, J.B. – Some Industrial Applications of Gamma-Ray Tomography – Journal of Taiwan institute of chemical engineers – Elsevier – 25 May 2009, pp 602 – 612.
- [16] Tortora, P.R., Ceccio, S.L., Mychkovsky, A.G., O’Hern, T.J., Torczynski, J.R. – Radial Profiles of Solids Loading and Flux in a Gas-Solid Circulating Fluidized Bed – AIChE JOURNAL – October 30, pp 5 – 6.
- [17] Kent (Hsin-Yu) Wei, Chang-Hua Qiu and Ken Primrose – Super-sensing technology: industrial applications and future challenges of electrical tomography – THE ROYAL SOCIETY – 28 June 2016, pp 3 – 4. <https://doi.org/10.1098/rsta.2015.0328>
- [18] Sharifi M, Young B – Electrical Resistance Tomography (ERT) applications to Chemical Engineering – Elsevier – September 2013, Vol 91, Iss 9, pp 1625 – 1645.
<https://doi.org/10.1016/j.cherd.2013.05.026>
- [19] Jan Porzuczek – Applications of electrical capacitance tomography for research phenomena occurring in the fluidized bed reactors – Chemical and process engineering 2014, 35(4), pp 397 – 408.
- [20] Yang, W. – Design of electrical capacitance tomography sensors – IOPSCIENCE – Measurement Science and Technology – 18 February 2010, Vol 21, pp 4 – 5.
- [21] I Ismail, J C Gamio, S F A Bukhari, W Q Yang - Tomography for multi-phase flow measurement in the oil industry – ELSEVIER – Flow measurement and

- instrumentation April 2005, Vol 16, Iss 2 – 3, pp 145 – 155,
<https://doi.org/10.1016/j.flowmeasinst.2005.02.017>.
- [22] A Parvareh, M Rahimi, A Alizadehdakhel, A A Alsairafi – CFD and ERT investigations on two-phase flow regimes in vertical and horizontal tubes – ELSEVIER – International Communications in Heat and Mass Transfer – March 2010, Vol 37, Iss 3, pp 304 – 311
<https://doi.org/10.1016/j.icheatmasstransfer.2009.11.001>.
- [23] Sharifi, M. and Young, B. – Electrical Resistance Tomography (ERT) applications to Chemical Engineering – ELSEVIER – Chemical Engineering Research and Design – September 2013, Vol 91, Iss 9, pp 1625 – 1645,
<https://doi.org/10.1016/j.cherd.2013.05.026>
- [24] G P Lucas, J Corry, R C Waterfall, W W Loh, F J Dickin – Measurement of the solids volume fraction and velocity distribution in solids-liquid flows using dual-plane electrical resistance tomography – ELSEVIER – Flow Measurement and Instrumentation – December 1999, Vol 10, Iss 4, pp 249 – 258,
[https://doi.org/10.1016/S0955-5986\(99\)00010-2](https://doi.org/10.1016/S0955-5986(99)00010-2).
- [25] R Giguere, L Fradette, D Mignon, P A Tanguy - ERT algorithms for quantitative concentration measurement of multiphase flows – ELSEVIER – Chemical Engineering Journal – 15 July 2008, Vol 141, Iss 1 – 3, pp 305 – 317
<https://doi.org/10.1016/j.cej.2008.01.011>.
- [26] Yousef Faraj - Measurement and Visualization of Slurry Flow Using Electrical Resistance Tomography – Doctoral Thesis – University of Leeds – March 2013, pp 55 – 56.
- [27] A M C Van Dinther, C G P H Schroen, F J Vergeldt – Suspension flow in microfluidic devices – ELSEVIER – Advance in Colloid and Interface Science - 15 May 2012, Vol 173, pp 23 – 34 <https://doi.org/10.1016/j.cis.2012.02.003>.
- [28] Dana Dabiri – Digital particle image thermometry/velocimetry – Springer-Verlag 2008 – Experiments in Fluids – December 2008

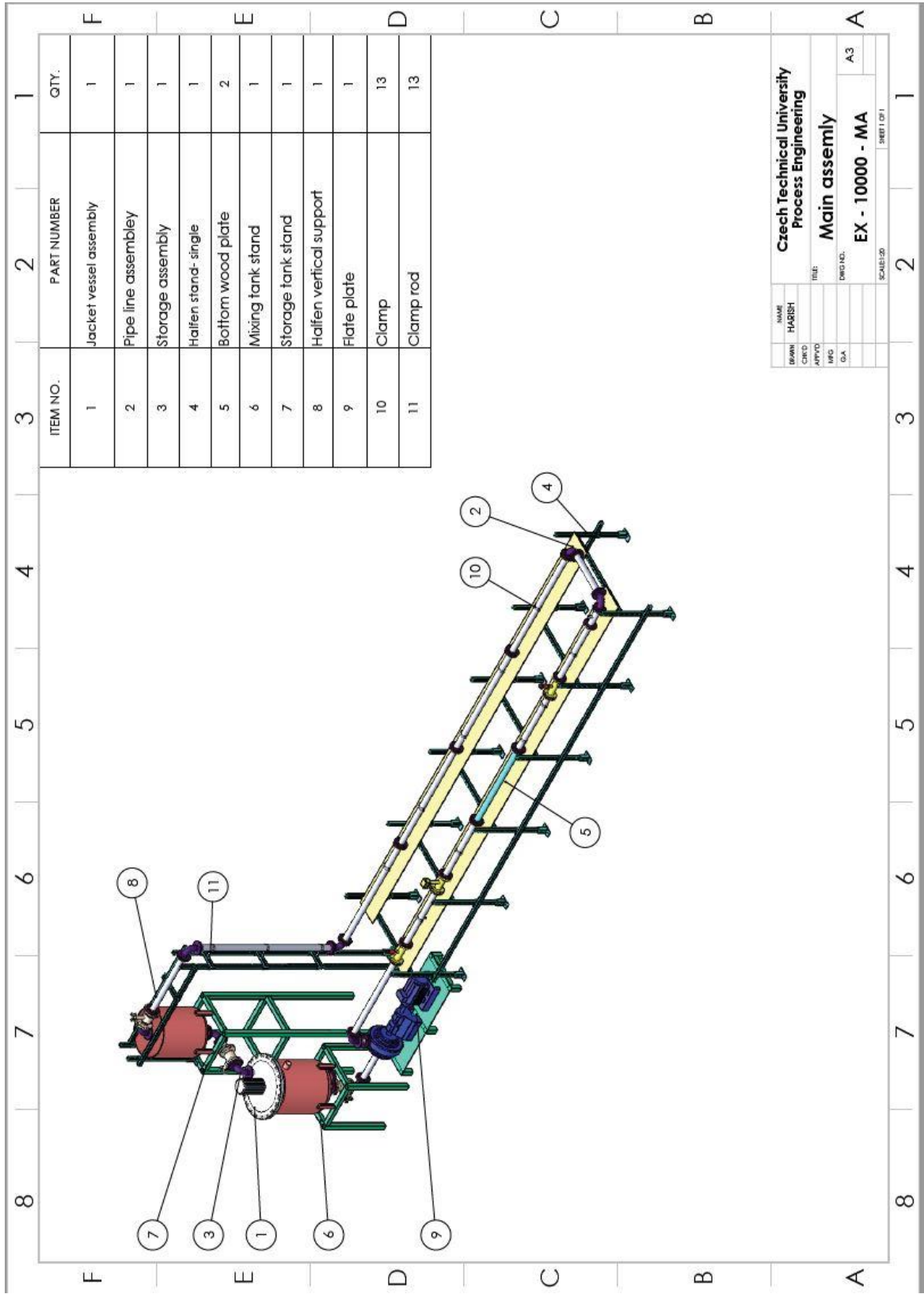
- [29] Carlomagno, G. M., Cardone, G., Meola, C., and Astarita, T – Infrared Thermography as a Tool for Thermal Surface Flow Visualization – Journal of Visualization – 1998, Vol 1, pp 37 – 50.
- [30] C. VerHulst, Jonathan Spirnak, Marc Samland, Brant Tremont, Alfred McQuirter, Elliott Williams, Michael Benson, Bret Van Poppel - Validation of Magnetic Resonance Thermometry through experimental and Computational approach – Aerospace Research Central – 22 July 2016.
- [31] Quan Zhou and Ke-Qing Xia – Comparative experimental study of local mixing of active and passive scalars in turbulent thermal convection – The Chinese University of Hong Kong – 13 November 2018.
- [32] Christie John Geankoplis, A. Allen Hersel Daniel H. Lepek (fifth edition) - Transport process and separation process and principles – New Jersey: Publishing as prentice Hall PTR – Fifth Edition – ISBN-13: 978-0-13-418102-8.
- [33] Karthick Ramisetty - Prediction of concentration profiles of a particles – Laden slurry flow in horizontal and vertical pipes – Bachelor Thesis – Jawaharlal Nehru Technological University – 2008.
- [34] Tecnofondi, Available from < <https://tecnofondi.it/en/products/dished-heads/dished-head-type-e/> >
- [35] C. Devarajulu and M. Loganathan – Effect of Impeller Clearance and Liquid Level on Critical Impeller Speed in an Agitated Vessel using Different Axial and Radial Impellers – Journal of Applied Fluid Mechanics – 2016, Vol 9, pp 2753 – 2761.
- [36] Pavel Ditl, Václav Novak – Dimensioning of the shaft of mixing devices – Czech Technical university – Prague.
- [37] Charles H. Forsberg– Average heat transfer coefficients – International; journal of Heat and Mass Transfer – Heat Transfer Principles and Applications – 2021.
- [38] Verein Deutscher Ingenieure VDI – Gesellschaft Verfahrenstechnik und Chemieingenieurwesen (GVC) Editor – VDI Heat Atlas – Second Edition – ISBN 978-3-540-77877-6.

- [39] TLV - A Steam Specialist Company. Available from:
< <https://www.tlv.com/global/TI/steam-theory/overall-heat-transfer-coefficient.html> >
- [40] NIST Chemistry WebBook – National institute of standards and technology – U.S. Department of commerce – 2021, <https://doi.org/10.18434/T4D303>
- [41] R. Patel, Udit Hansalia, Manan Modi, Rahul Patel, Krunal Parikh – Design and Fabrication Of Tube In Tube Heat Exchanger – International Research Journal of Engineering and Technology – April 2021, Vol 08, Issue 4, pp 1784 – 1785.
- [42] NPTEL – Process design of Heat Exchangers – Chemical Engineering – Chemical Engineering Design – II.
- [43] Jacket vessels types - <https://www.sigmathermal.com/applications/jacketed-vessels/>.
- [44] ASME pressure vessel jacket types - R-V Industries INC.
- [45] C.E., Perkins, J., Schmit, Eldridge, R.B – Investigation of X-ray imaging of vapor-liquid contactors. 2. Experiments and simulations of flows in an air-water contactor – Elsevier – Chemical Engineering Science – 2004, pp 1267 – 1283.
- [46] Sharad N. Pachpute (PhD. IIT Delhi), ‘CFD Flow Engineering’ Slurry flow and its CFD Modelling.
- [47] Experimental stand for testing flow conditions. [Dwg.No. EX-10000-MA]
- [48] Bereich von, Masdom Measurement methods- LDA, 2012 Available from <<http://141.44.132.124:8080/masdom/measurement-method/lda>>
- [49] Huai Z. Li, Nicolas Dietrich, Souhila Poncin, ‘Dynamic deformation of a flat liquid-liquid interface. Springer – Verlag 2010.
- [50] David J.Parker, Xianfeng Fan , Positron emission particle tracking-Application and labelling techniques. Science direct – 2008
- [51] M. Messer, Plused ultrasonic doppler velocimetry for measurement of velocity profiles in small channels and capillaries. Semantic scholar – 2005.

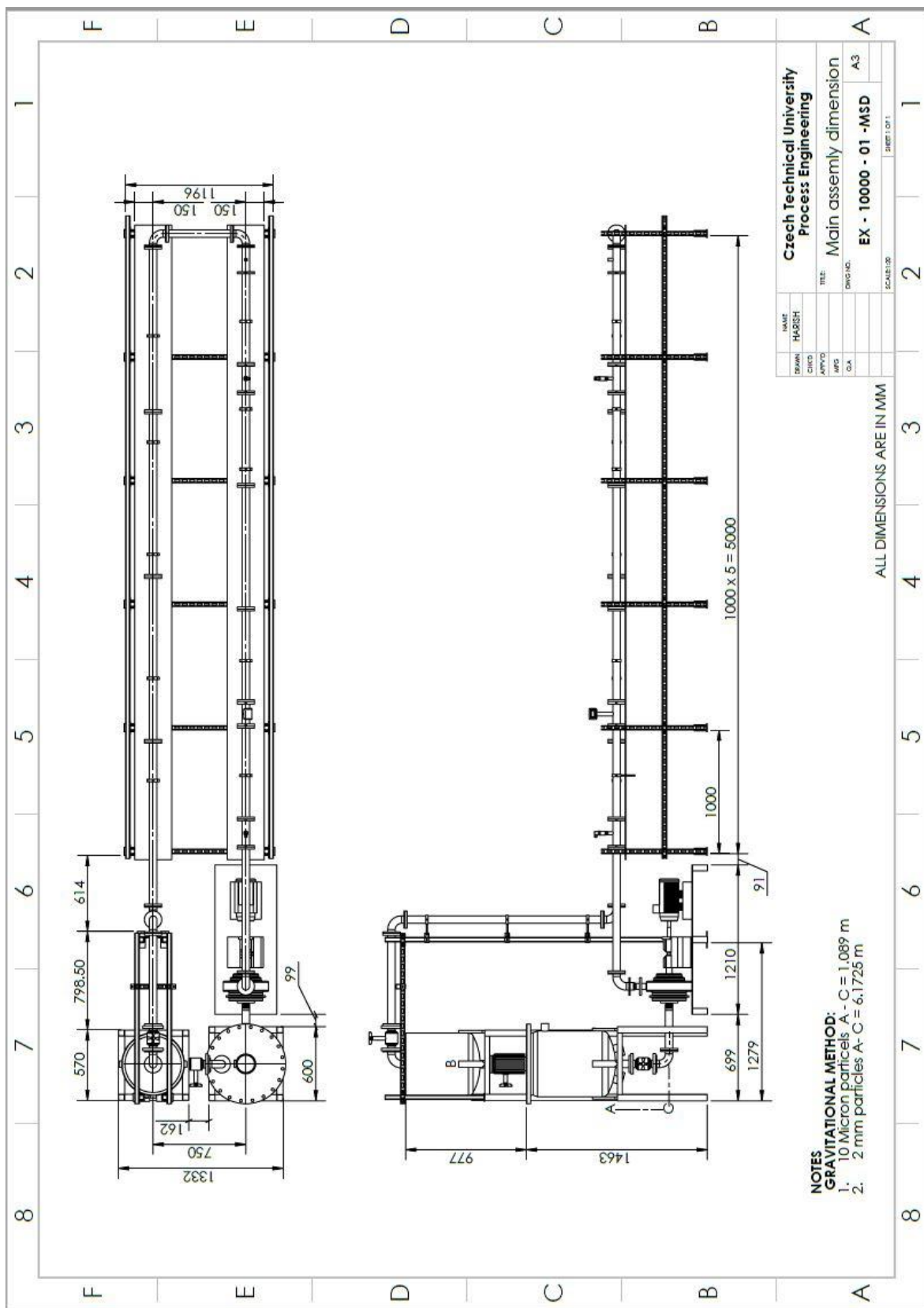
- [52] R.F. Mudde, Advanced measurement techniques for GLS reactors. Wiley online library -2015.
- [53] Xuekai, Yadan Jiang, Baoliang Wang and Zhiyao Huang, On the performance of a capacitively coupled electrical impedance tomography sensor with different configurations. ‘Tomography Sensing Technique’ – 2020.
- [54] I. Ismail, A. Jaafar. Areeba Shafquet. Application of Electrical Capacitance Tomography on single – plane sensor measurement, 2013.
- [55] I. Ismail, J.C. Gamio, Tomography for multiphase flow measurement in oil industry, 2005.
- [56] Suzanna Ridzuan Aw, Chiew Loon Goh, Electrical resistance tomography a review of the applications of conducting vessel walls, 2014
- [57] K. W. Moser, E. C. Kutter, J.G. Georgiadis, R.O. Buckius, H. D. Morris, J. R. Torczynski, Velocity measurement of flow through a step stenosis using Magnetic Resonance Imaging, 1999.
- [58] Agitation and mixing of fluids. Available from
<http://users.fs.cvut.cz/~jiroutom/huo_soubory/huo8a.pdf>
- [59] Vector Stock – OstapGor. Available from < <https://www.vectorstock.com/royalty-free-vector/cut-double-pipe-heat-exchanger-apparatus-vector-25182303> >
- [60] The piping Talk – July 2021. Available from < <https://thepipingtalk.com/types-of-heat-exchanger-according-to-construction> >
- [61] Arya Sepher Kayhan – Pump & Electro power system. Available from
<<http://www.aryask.com/oh1-series.html>>
- [62] ABB – Drive and motor selection. Available from
<<https://selector.drivesmotors.abb.com/recommended-drives#tabSection>>
- [63] Danfoss – Sensing solutions. Available from
<https://store.danfoss.com/gb/en_GB/Sensing-Solutions/Pressure-Transmitters/Pressure-Transmitters%20A0/Pressure-transmitter%2C-MBS-4010%2C-0-00-bar---4-00-bar%2C-0-00-psi---58-02-psi/p/060G3211>

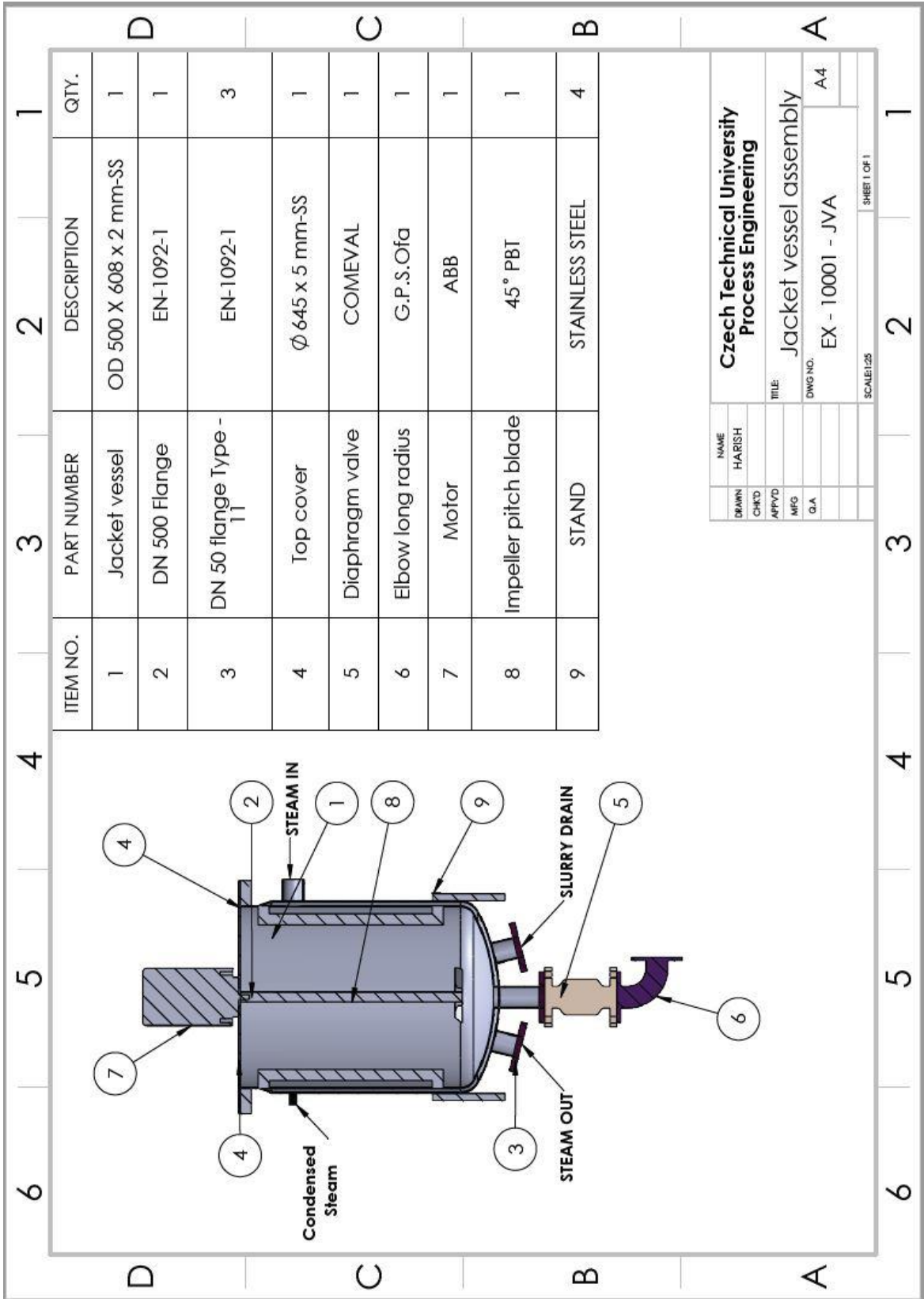
- [64] Siemens – Products & service Available from
<<https://new.siemens.com/global/en/products/automation/process-instrumentation/flow-measurement/electromagnetic/sitrans-f-m-mag-3100.html> >
- [65] Diaval – Diaphragm valves. Available from
<https://www.comeval.es/products/DS/diaphragm_valves_straight_through_type-st-diaval-data_sheet-en-ds09_s.pdf >
- [66] JAKAR Electronics. Available from < <https://www.jakar.cz/en/p/k-type-thermocouple-duplex-wire#3133> >
- [67] Vocaldo J J and Charles M E – Prediction of pressure gradient for the horizontal turbulent flow of slurries – In Proc. 2nd Int. Conf. on the Hydraulic Transport of Solids in Pipes – 1972 – Paper C1, pp. 1-12.
- [68] Gui L and Merzkirch W – Phase-separated PIV measurements in two-phase flow by applying a digital mask technique. ERCOFTAC Bulletin 30 – 1996, pp 45 – 48.
- [69] S Funatani, N Fujisawa and H Ikeda – Simultaneous measurement of temperature and velocity using two-colour LIF combined with PIV with a colour CCD camera and its application to the turbulent buoyant plume – INSTITUTE OF PHYSICS PUBLISHING – 20 April 2004 - Measurement Science and Technology, Volume 15, Number 5 – <https://iopscience.iop.org/article/10.1088/0957-0233/15/5/030>

Appendices



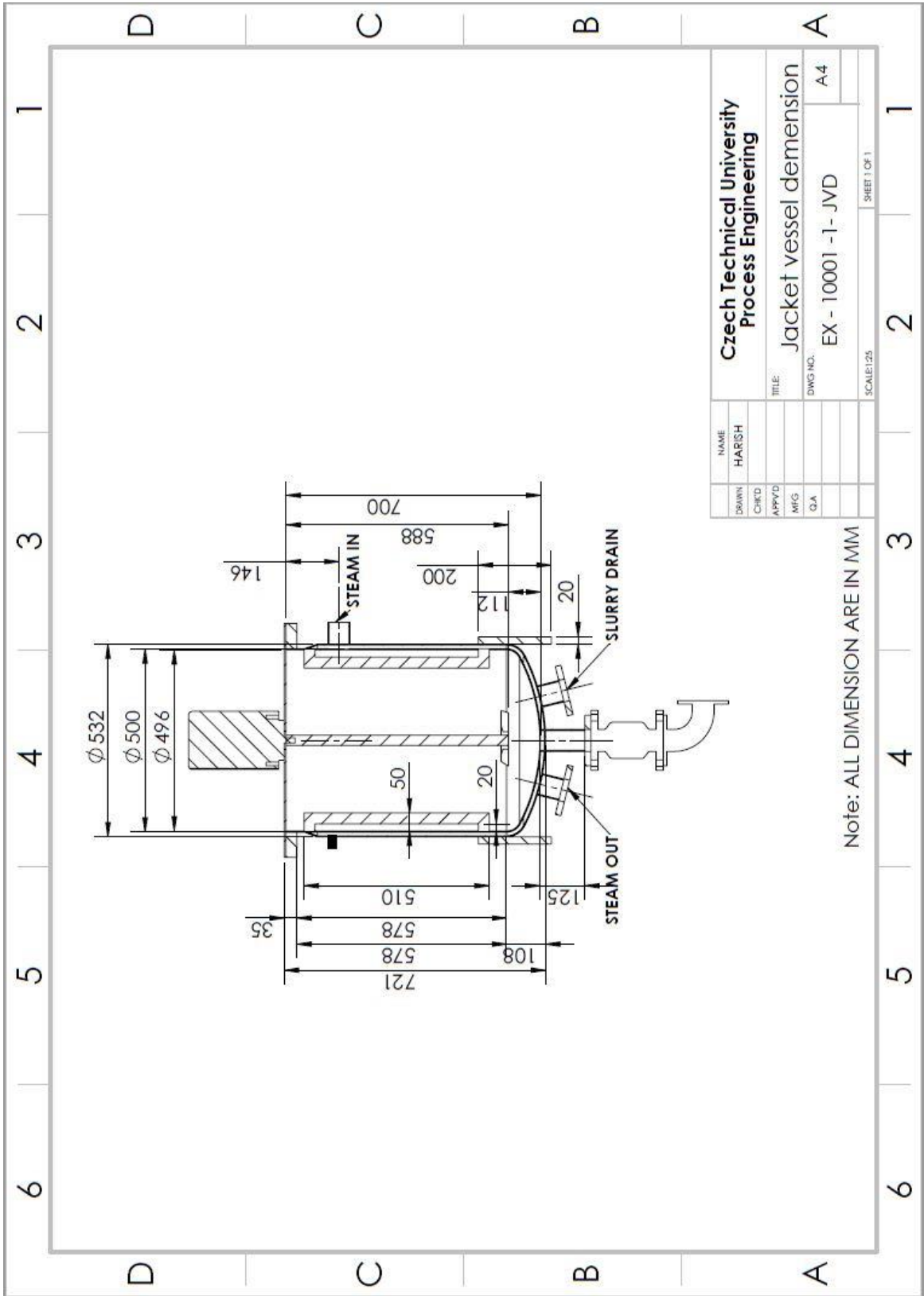
NAME	HABESH
BRWN	
CRKD	
APPRO	
INFC	
QA	
TITLE	Czech Technical University Process Engineering
DWG NO.	Main assembly
SCALE	EX - 10000 - MA
SHEET NO.	A3
SHEET OF	1



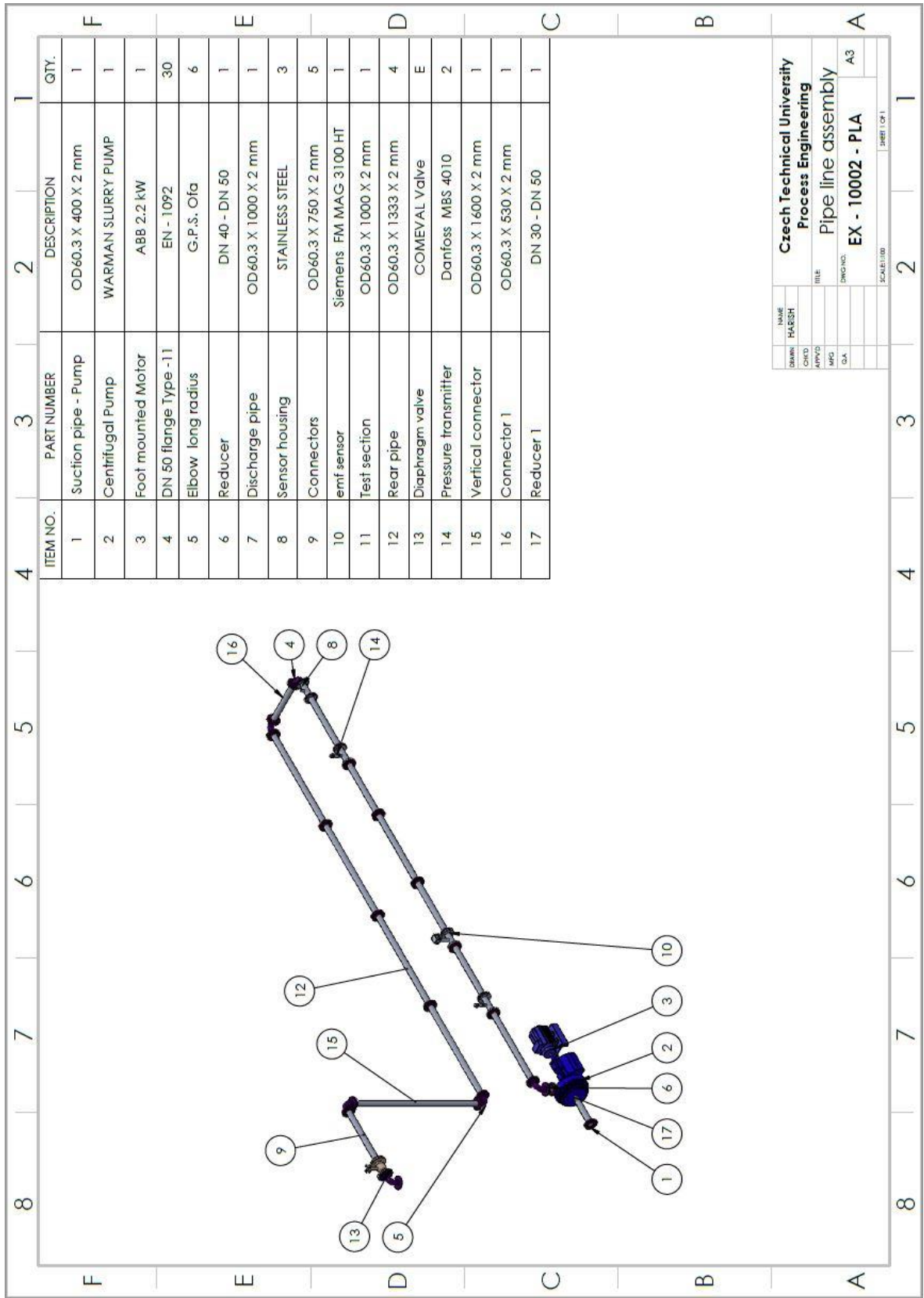


ITEM NO.	PART NUMBER	DESCRIPTION	QTY.
1	Jacket vessel	OD 500 X 608 x 2 mm-SS	1
2	DN 500 Flange	EN-1092-1	1
3	DN 50 flange Type - 11	EN-1092-1	3
4	Top cover	Ø 645 x 5 mm-SS	1
5	Diaphragm valve	COMEVAL	1
6	Elbow long radius	G.P.S.Ofa	1
7	Motor	ABB	1
8	Impeller pitch blade	45° PBT	1
9	STAND	STAINLESS STEEL	4

NAME	HARISH
DRAWN	
CHKD	
APPRD	
MFG	
D.A.	
Czech Technical University Process Engineering	
TITLE:	Jacket vessel assembly
DWG NO.	EX - 10001 - JVA
	A4
SCALE:1:25	SHEET 1 OF 1

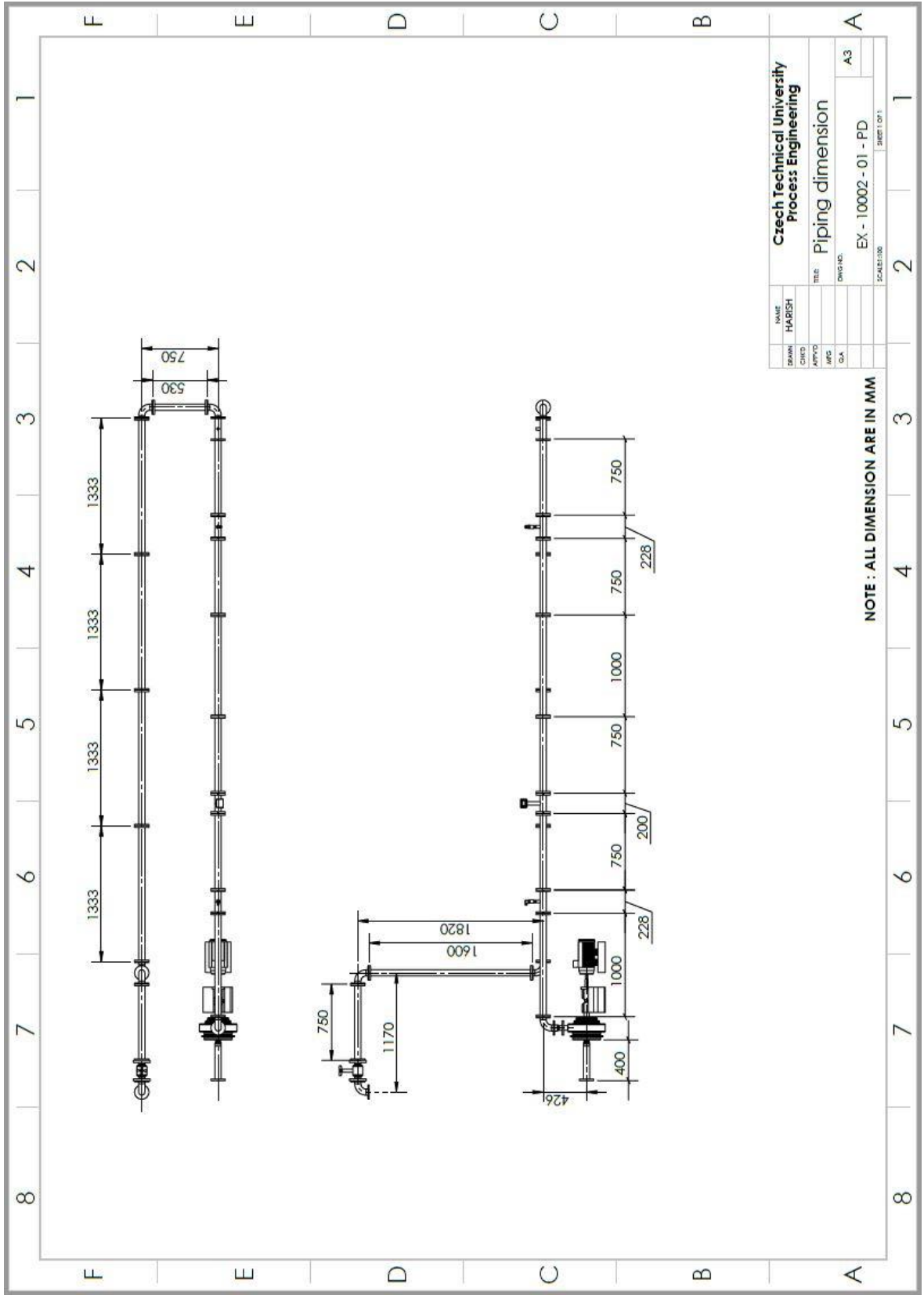


NAME	HARISH
DRAWN	
CHKD	
APPVD	
MFG	
QA	
TITLE	Jacket vessel demension
DWG NO.	EX - 10001 -1- JVD
SCALE:1:25	A4
SHEET 1 OF 1	



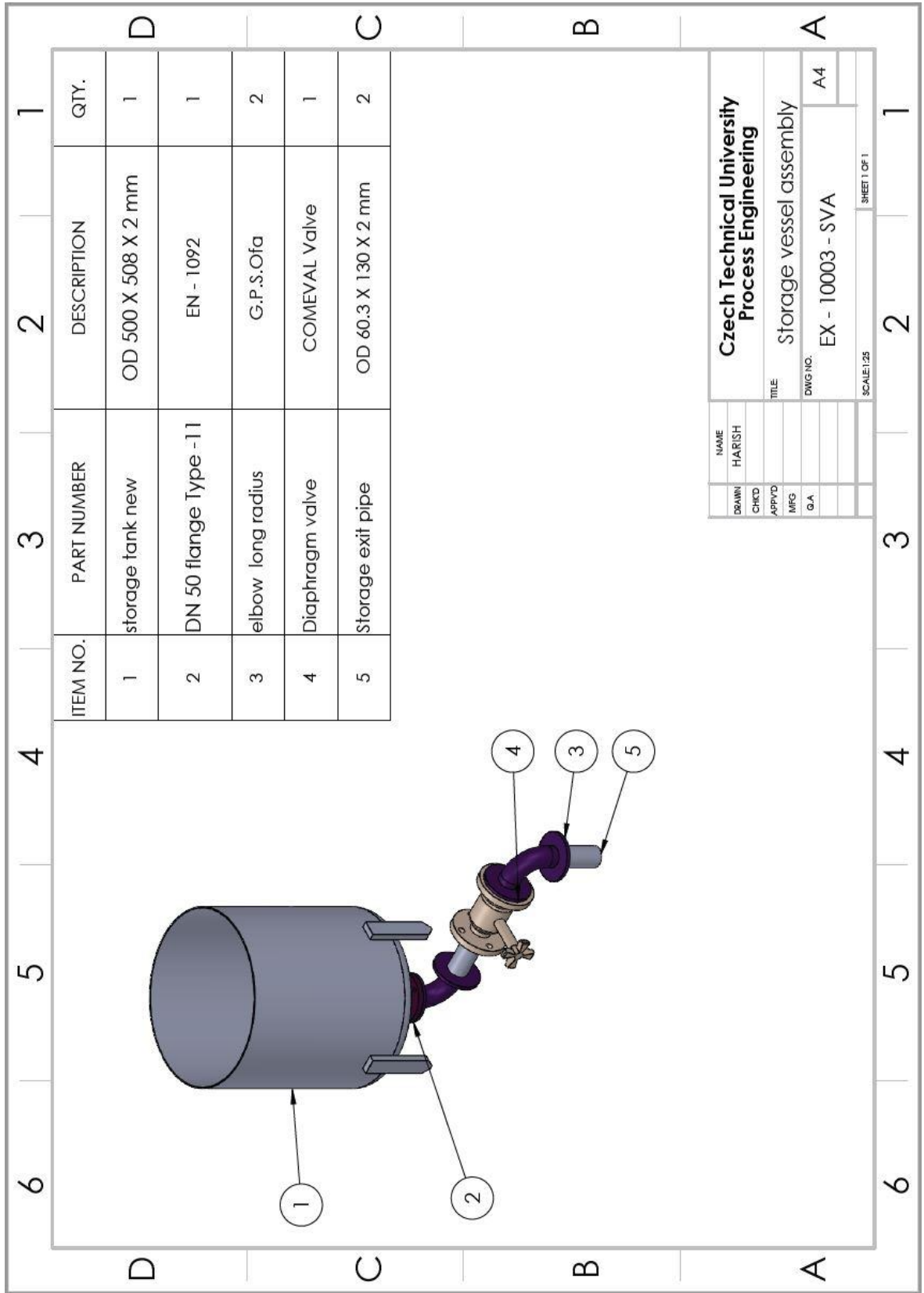
ITEM NO.	PART NUMBER	DESCRIPTION	QTY.
1	Suction pipe - Pump	OD60.3 X 400 X 2 mm	1
2	Centrifugal Pump	WARMAN SLURRY PUMP	1
3	Foot mounted Motor	ABB 2.2 kW	1
4	DN 50 flange Type -11	EN - 1092	30
5	Elbow long radius	G.P.S. Ofa	6
6	Reducer	DN 40 - DN 50	1
7	Discharge pipe	OD60.3 X 1000 X 2 mm	1
8	Sensor housing	STAINLESS STEEL	3
9	Connectors	OD60.3 X 750 X 2 mm	5
10	emf sensor	Siemens FM MAG 3100 HT	1
11	Test section	OD60.3 X 1000 X 2 mm	1
12	Rear pipe	OD60.3 X 1333 X 2 mm	4
13	Diaphragm valve	COMEVAL Valve	E
14	Pressure transmitter	Danfoss MBS 4010	2
15	Vertical connector	OD60.3 X 1600 X 2 mm	1
16	Connector 1	OD60.3 X 530 X 2 mm	1
17	Reducer 1	DN 30 - DN 50	1

NAME	HARISH
DRAWN	
CHECKED	
APPROVED	
MFG	
QA	
Czech Technical University Process Engineering	
TITLE Pipe line assembly	
DWG NO.	EX - 10002 - PLA
SCALE	A3
SHEET 01/1	

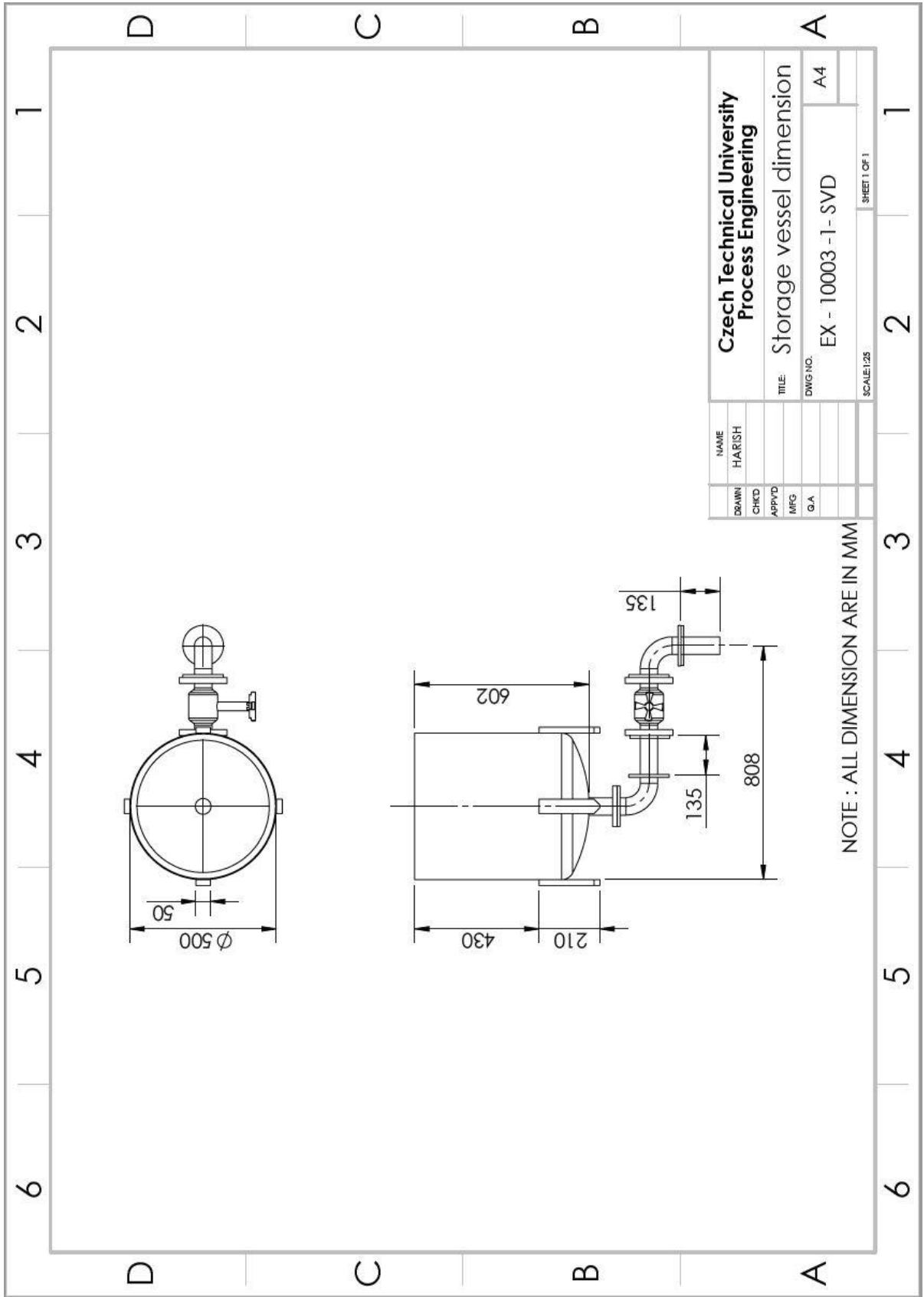


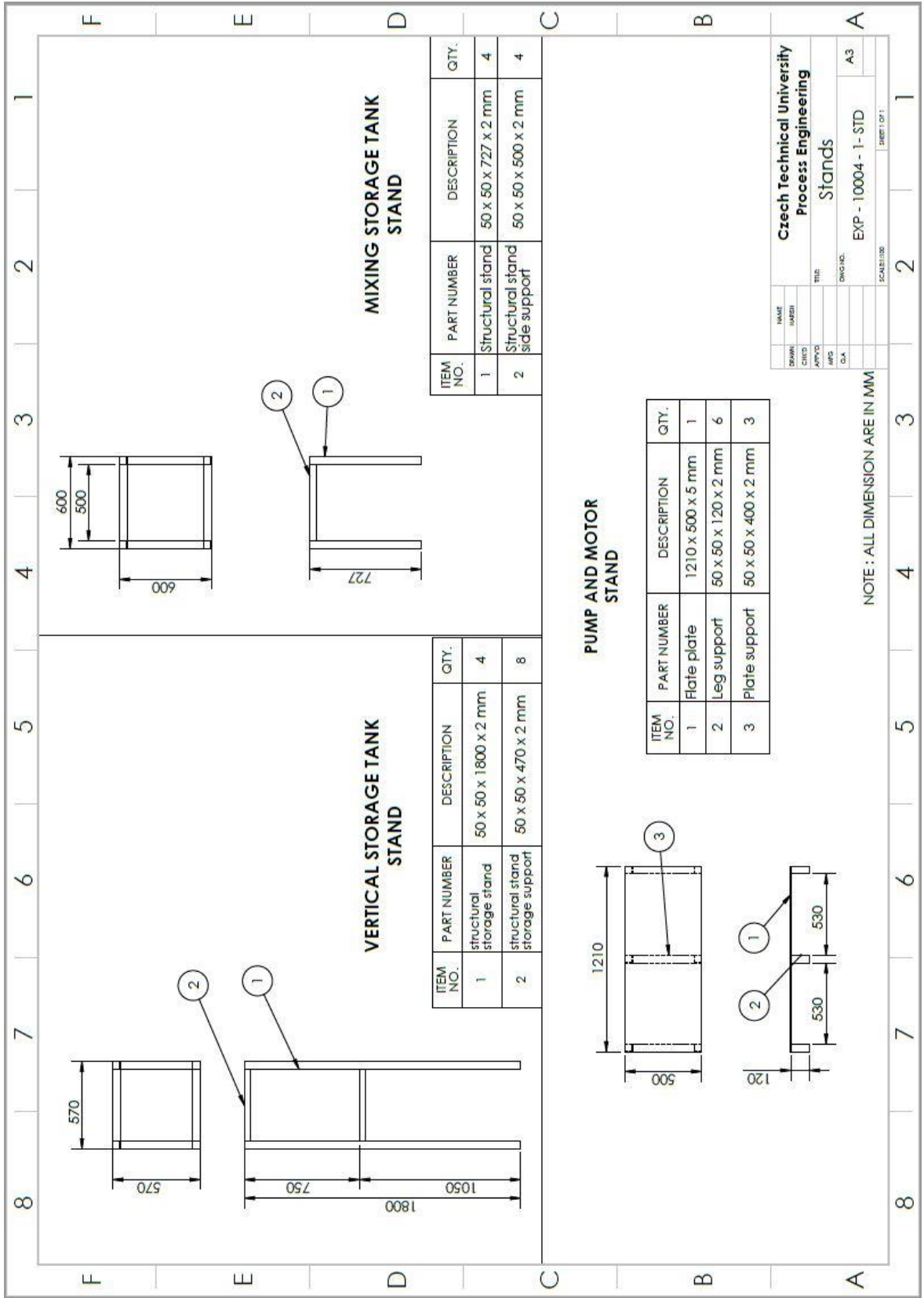
NOTE : ALL DIMENSION ARE IN MM

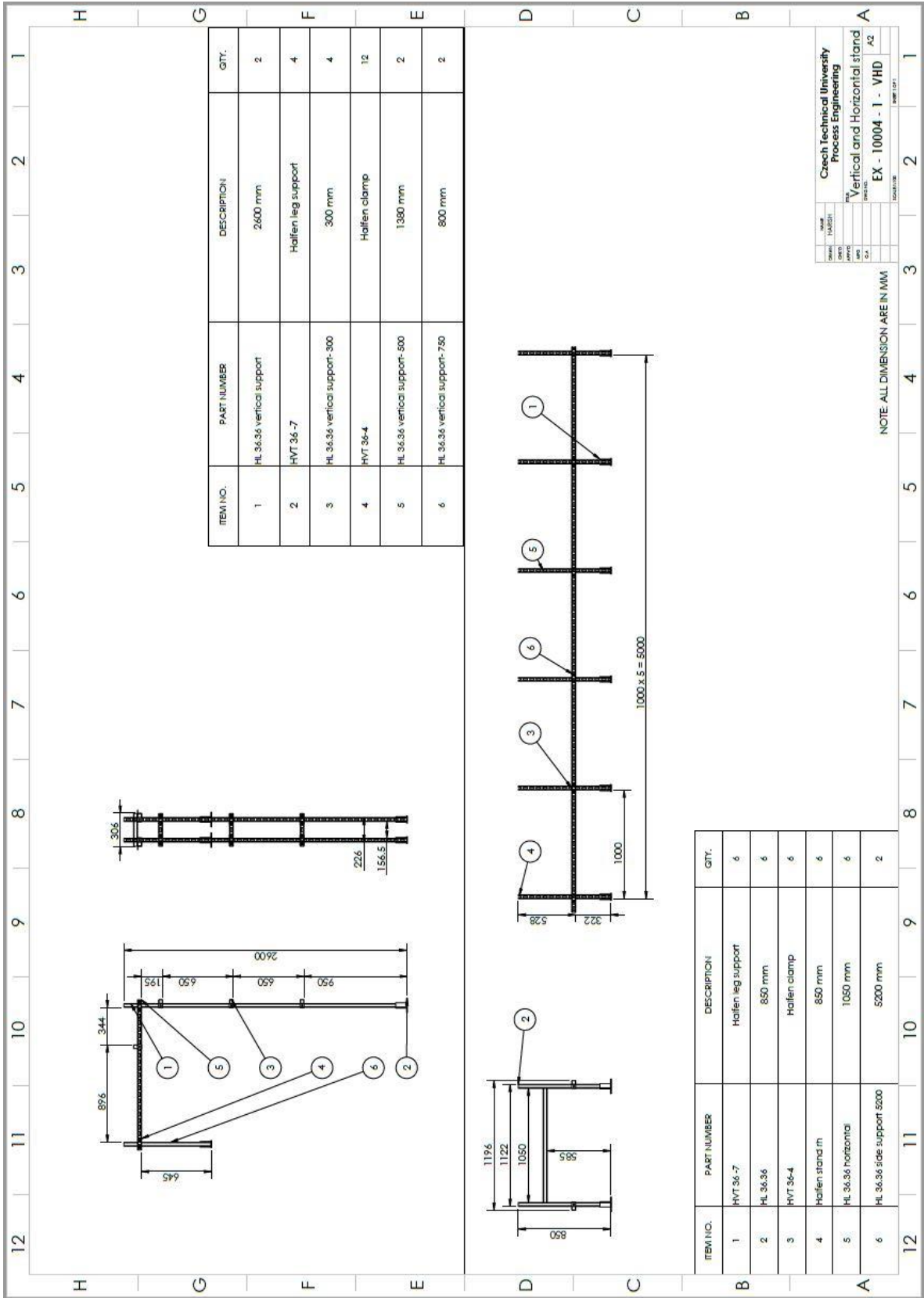
NAME	HARISH
DRWN	
CHCK	
APP'D	
APP'D	
Q.A.	
Czech Technical University Process Engineering	
TITLE	Piping dimension
DRWG NO.	EX - 10002 - 01 - PD
SCALE	1:1
SHEET NO.	A3
SHEET 1 OF 1	



NAME	HARISH
DRAWN	
CHKD	
APPVD	
MFG	
G.A	
TITLE	
Storage vessel assembly	
DWG NO.	EX - 10003 - SVA
	A4
SCALE:1:25	
SHEET 1 OF 1	







Czech Technical University
 Process Engineering
 Vertical and Horizontal stand
 EX - 10004 - 1 - VHD 22